# INVESTIGATIONS ON POWER CONVERTER TOPOLOGIES FOR RENEWABLE ENERGY APPLICATIONS

## A DISSERTATION

*Submitted in partial fulfillment of the*
*requirements for the award of the degree*
*of*
**INTEGRATED DUAL DEGREE**
In
**ELECTRICAL ENGINEERING**
(With Specialization in Power Electronics)

By
**ISHITVA MAITRAY**


**DEPARTMENT OF ELECTRICAL ENGINEERING**
**INDIAN INSTITUTE OF TECHNOLOGY ROORKEE**
**ROORKEE – 247 667 (INDIA)**
**MAY, 2016**

# CANDIDATE'S DECLARATION

I hereby declare that the work presented in the dissertation report entitled "**Investigations on Power Converter Topologies for Renewable Energy Applications**" submitted in partial fulfillment of the requirements for the award of the degree of Integrated Dual Degree in Electrical Engineering with Specialization in Power Electronics, submitted in the Department of Electrical Engineering, Indian Institute of Technology, Roorkee is an authentic record of my work carried out under the guidance and supervision of Dr. Mukesh K. Pathak, Associate Professor, Department of Electrical Engineering, Indian Institute of Technology, Roorkee.

Date:

Place: Roorkee (Ishitva Maitray)

# CERTIFICATE

This to certify that the above statement made by the candidate is correct to the best of my knowledge.

Dr. Mukesh K. Pathak
Associate Professor
Department of Electrical Engineering
Roorkee – 247667, India Indian Institute of Technology, Roorkee

# ABSTRACT

Renewable energy sources are gaining popularity due to shortcomings of conventional sources of energy. Solar power is considered a very promising source for electric power generation. The abundance of sunlight over a large area of the earth surface gives rise to several applications of photovoltaic systems. These systems are widely used today to provide power to either standalone loads or for connection to the power system grid. Integration of PV generators with power system grid is presented in this work.

There has been a phenomenal development in the area of power converter topologies for PV systems. Two level and three level voltage source inverters are amongst the most popular topologies for grid connected systems. Investigation of load and insolation based variations are studied for these two topologies.

Maximum power point tracking (MPPT) is a very important consideration that is taken into account when building a new photovoltaic power system. This is needed in order to extract maximum power output from a PV array under varying atmospheric conditions to maximize the return on initial investments. In dual stage PV system boost DC-DC converter is responsible for this particular function. There is also a need for developing control techniques for three phase grid connected PV systems including a method for DC link voltage control that can stabilize the voltage at the inverter input. Control of injected current is also essential for unity power factor operation.

Simulation of the designed PV system has been carried out in MATLAB and effects of change in conditions have been investigated for two topologies in consideration.

# ACKNOWLEDGEMENT

This report is the result of the project “Investigations on Power Converter Topologies for Renewable Energy Applications” for the partial fulfillment of the Master of Technology in Electrical Engineering. I wish to affirm my deep sense of gratitude to my guide Dr. Mukesh Pathak, Department of Electrical Engineering, IIT Roorkee for intuitive and meticulous guidance in completion of this seminar report. I want to express my profound gratitude for his genial and kind co-operation in completing this work and his valuable suggestions throughout the work.

I convey my gratitude to Dr. S. P. Srivastava, Head of Department, Electrical Engineering, IIT Roorkee for providing me this opportunity to pursue this project. I also acknowledge the blessings of my parents for encouragement and moral support rendered to me throughout my life.

I humbly acknowledge the help of all those who were involved directly or indirectly with my dissertation work.

# LIST OF FIGURES

# LIST OF ACRONYMS

| | |
|---|---|
| AC | Alternating Current |
| DC | Direct Current |
| DCMLI | Diode Clamped Multi Level Inverter |
| FFT | Fast Fourier Transform |
| IGBT | Insulated Gate Bipolar Transistor |
| MLI | Multilevel Inverter |
| MOSFET | Metal Oxide Semiconductor Field Effect Transistor |
| MPPT | Maximum Power Point Tracking |
| NPC | Neutral Point Clamped |
| PI | Proportional Integral |
| PLL | Phase Locked Loop |
| PWM | Pulse Width Modulation |
| PV | Photovoltaic |
| SPWM | Sinusoidal Pulse Width Modulation |
| THD | Total Harmonics Distortion |
| TPBI | Three Phase Bridge Inverter |
| VSI | Voltage Source Inverter |

# TABLE OF CONTENTS

# Chapter 1: INTRODUCTION

The aim of this chapter is to provide the research motivations related to the study and the objectives to be reached from it. The literature used has been reviewed critically. An outline is presented as well to give a summary of the topics covered in each chapter.

## 1.1. Research Motivation

***The World Energy Consumption***

Demand for energy has increased exponentially in recent years. In [3], the world energy consumption is expected to rise by 49 percent from 2007 to 2030 as shown in Figure 1.1. The development of economies is heavily dependent on energy resources. The growth of human population is projected from 6.1 billion in 2000 to 8.9 billion in 2050 [2], and energy is the essential element to maintain the pace of development of the human race.

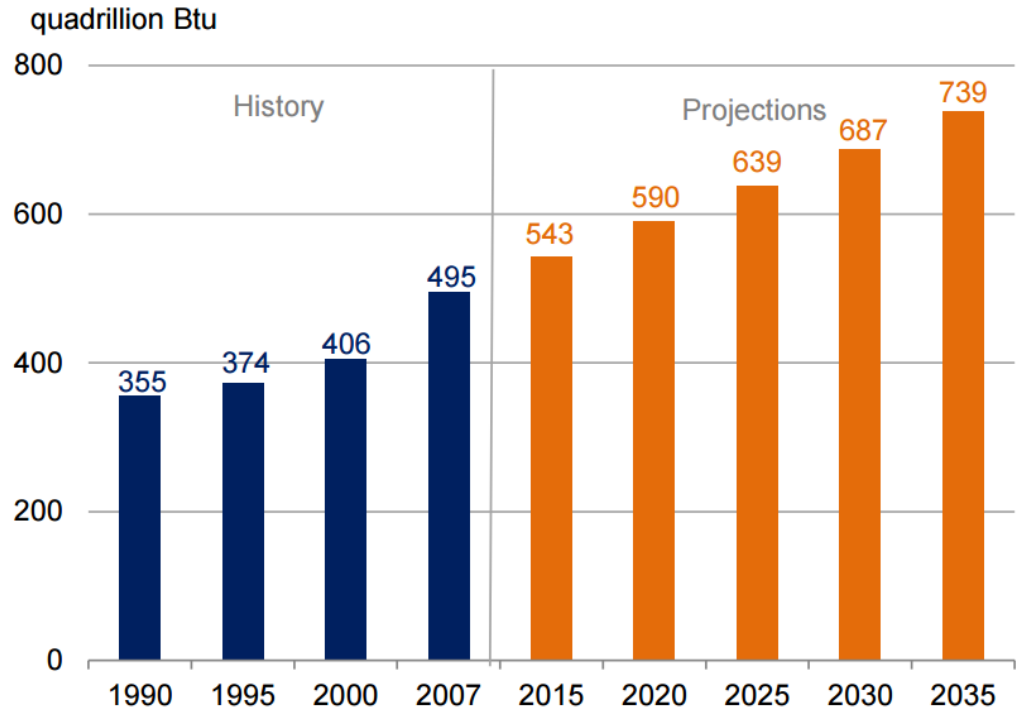


Figure 1.1: World Energy demand trend

In the increase of energy consumption, fossil fuel -liquids, coal and natural gas- will remain the largest and the world dominant source of energy for the predictable future [4]. While liquid fuels are expected to remain the prevalent source of energy since their outstanding role in the transportation and industrial areas, the liquids consumption is estimated to decline from 35 percent in 2007 to 30 percent in 2030 [2]. On global basis the use of liquids fuel decreases in the electric power area as electricity generators trying to switch to alternative fuels as the oil prices is gradually rising.

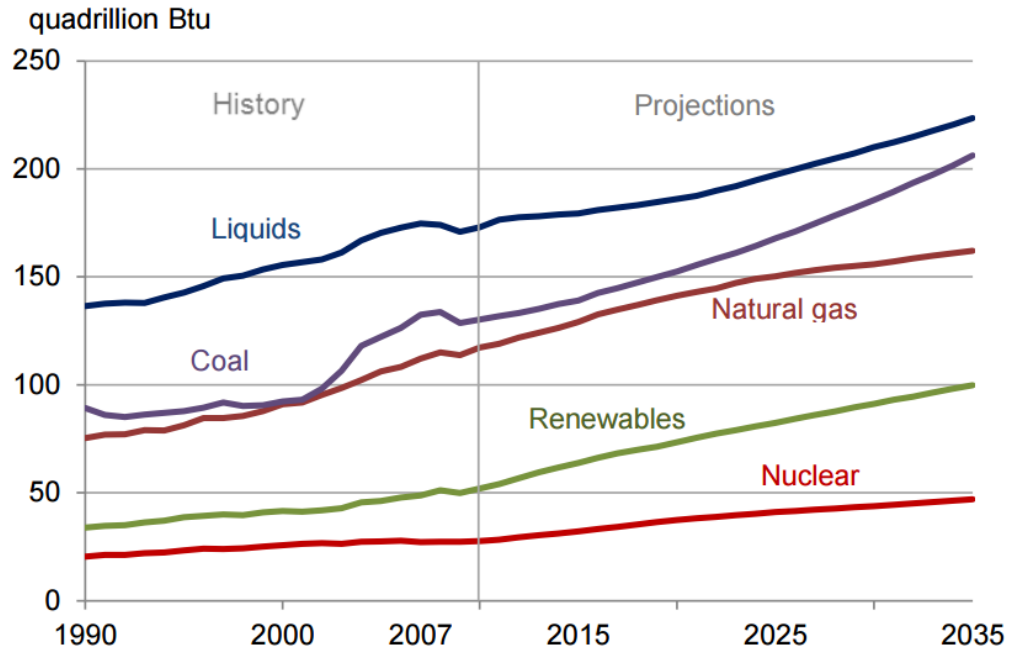


Figure 1.2. World marketed energy consumption, 1990-2035 [1].

World net electricity generation is projected to increase from 18.8 trillion kilowatt-hours in 2007 to 35.2 trillion kilowatt-hours in 2035 which is 2.3 percent per year [2]. Worldwide, the assortment of fuel source to generate electricity has been changed over past four decades.

Coal is still the main source for generating electricity and is projected to fuel the largest portion of electricity in the next two decades. But since coal is the most carbon dioxide intensive source of energy, national concern about greenhouse gas emission is forcing countries toward using less carbon-intensive sources.

Natural gas is another source of energy used to produce electricity which is less carbon intensive compare to coal and liquid fuel. Electricity generated by natural gas is

cheaper than oil. Also natural gas fired power plants are less expensive compared to power plants that use coal, nuclear and also most renewable energy power plants [2]. It has the ability to be used in combined-cycle fired power which is efficient. It also gives the dispatch controller the ability to bring the power plant online in few minutes, and in turn it takes several hours for coal fired power plants.

On the global basis, liquid fuels are the only energy source of electricity which does not grow. Beside its environmental effect, the rising price of liquid fuels and the energy security concern are the reasons that countries are moving towards reducing their use of oil and alternate it with cheaper sources like coal and nuclear. The reasons that are mentioned in previous paragraph are what keeps the liquids fuel's growth from increasing, and is drawing new attention to nuclear power plants in recent years. But concerns about its safety, radioactive waste disposal and investment risk make the countries cautious about implementing nuclear plants.

***Renewable Energy***

Renewables are the fastest-growing source of world energy, with consumption increasing by 3.0 percent per year (Figure 1.2 and 1.3). World concern about global warming and the fact that fossil fuel affect global environment through air pollution and greenhouse gas emission push the international society toward using alternative sources like renewable energy.

Renewable energy uses natural systems and cycles such as sunlight, wind, tides, and geothermal heat to create energy. The main obstacle to developing renewable energy sources is cost. Economically, most renewable technologies cannot compete with fossil fuels. However, the cost of operating renewable sources like solar and wind once they are built is much lower than those of fossil fuel power plants.

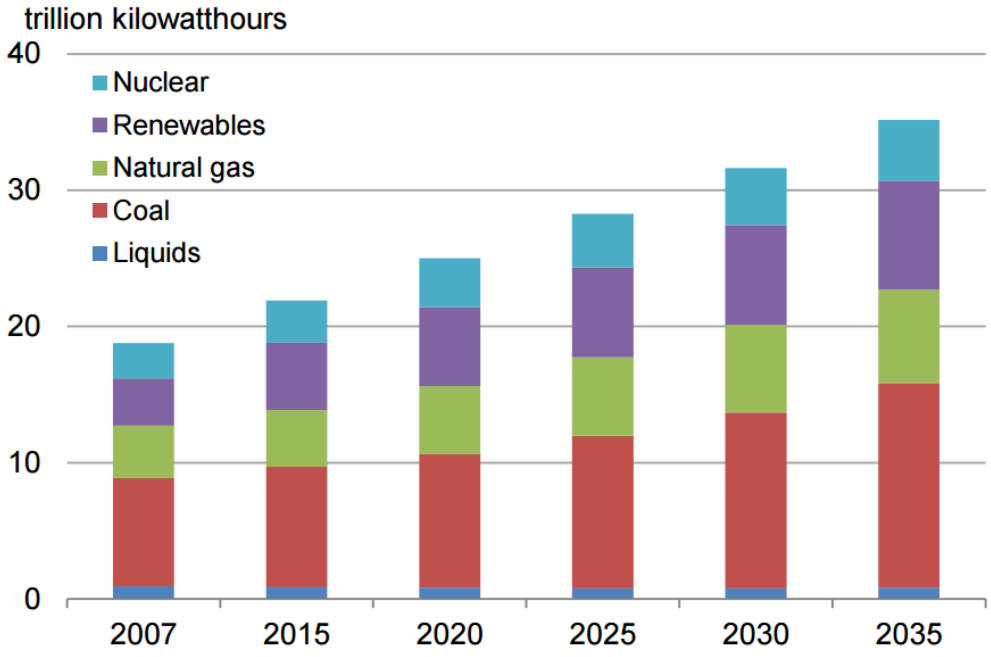


Figure 1.3. World electricity generation by fuel, 2007-2035 [1].

***Solar Energy***

Solar power technology or photovoltaic (PV), which is non-thermal solar conversion technology, generates electricity directly from radiation. PV based systems are growing rapidly. Grid-connected PV capacity has increased 60 percent from 2004 to 2015 [5]. PV has little operational maintenance. However solar energy is still expensive and cannot compete with fossil fuels despite the development of technology and improvement of its efficiency. Solar power is a niche of renewable energy but it can be economical where electricity prices goes up or where government incentives are provided. Currently, lots of research is being done on solar power since governmental policies is to support renewable energy, especially solar power [3].

Given the limitations of continued use of conventional sources of energy, renewable energy sources are becoming more popular. One of such most promising application is grid integration of photovoltaic energy modules in order to harness abundant solar energy.

In PV systems connected to the grid, the inverter which converts the output direct current (DC) of the solar modules to the alternate current (AC) is receiving increased interest in order to generate power to utility. Many topologies are used to this purpose. This study

aims at investigating three popular power inverter topologies and related control structures for grid connected photovoltaic systems.

## 1.2. Research Objectives

The goal of this study is to investigate different inverter topologies for grid connected photovoltaic system. In this work, two and three level Voltage Source Inverter Topologies are investigated. Both the topologies are part of a dual power stage PV system. Following points presents the scope of this work:

- Formulation of research problem by study and literature review of grid connected PV system and related topologies. Development of conceptual background on two level and three level VSI topologies, system components and control structures to be used.
- Mathematical modeling of the PV array to study the various characteristics of the PV array and the effect of the irradiance and temperature on the performance of the PV array along with algorithms to extract the maximum power from the PV panel under varying environmental conditions of irradiance and temperature.
- Development of control strategy for three phase grid connected PV system including control of grid voltages and injected currents, and generating gating pulses for inverters.
- Simulations of the developed systems using MATLAB Simulink environment. Investigation of inverter performance for both topologies using customized simulation timeline of events.
- Attempt to develop a hardware prototype of three phase grid connected PV system using two level inverter.

## 1.3. Literature Review

*M. G. Villalva* (2009) presented comprehensive Approach to Modeling and Simulation of Photovoltaic Arrays.

A detailed Comparison of Photovoltaic Array Maximum Power Point Tracking Techniques was presented by *T. Esram and P. L. Chapman* (2007).

*Hussein, K.H; Muta I; Hoshino, T; Osakada, M.* (2001) analyzed maximum photovoltaic power tracking algorithms response to rapidly changing atmospheric conditions.

A study on a two stage maximum power point tracking control of a photovoltaic system under partially shaded insolation conditions was conducted by *K. Kobayashi, I. Takano, and Y. Sawada (2003).*

*Kroutikova, N.; Hernandez-Aramburo, C.A.; Green, T.C* (2007) presented different state-space model of grid-connected inverters under current control mode.

Overview of control and grid synchronization for distributed power generation systems was done comprehensively by *F. Blaabjerg* (2004)..

*M. P. Kazmierkowski and L. Malesani* (2007) surveyed current control techniques for three-phase voltage source PWM converters.

## 1.4. Dissertation Outline

The dissertation is comprised of five chapters. Each chapter discuss a particular aspect of VSI topologies based grid connected photovoltaic system in detail.

**Chapter 1** is an introductory chapter that covers motivation for this project, literature survey, research objectives and presents an outline for subsequent chapters.

**Chapter 2** lucidly explains Voltage Source Inverter topologies used in proposed grid connected photovoltaic system. Circuit operation and control strategy employed are explained in detail.

**Chapter 3** presents a concise description of the three phase grid connected photovoltaic system. Various components of the system are described comprehensively. Exhaustive explanation of the PV inverter control scheme is also given.

**Chapter 4** contains system simulations performed in MATLAB along with simulation results. Clear explanations and related inferences of simulation results for both VSI topologies are presented.

**Chapter 5** discusses system hardware development for grid connected two level VSI. Different components of the system are tested. Scope for future work is included as well.

**Chapter 6** presents conclusion and further recommendations.

# Chapter 2: INVERTER TOPOLOGIES

This chapter gives a detailed description of three VSI topologies used in three phase grid connected PV system. VSI is used as DC-AC grid interface in the system, thus making the controlled transfer of active power from PV generator to the grid possible. Inverter circuit operation along with the control strategy employed are explained comprehensively. Sine Pulse Width Modulation (SPWM) control technique is used in all three cases.

## 2.1. Two level Three Phase Bridge Inverter

### 2.1.1. Inverter circuit

Voltage source inverters (VSI) are mainly used to convert a constant DC voltage into 3-phase AC voltages with variable magnitude and frequency. Fig 2.1 shows a schematic diagram of a three phase VSI. The inverter is composed of six switches S1 through S6 with each phase output connected to the middle of each "inverter leg". Two switches in each phase are used to construct one leg. The AC output voltage from the inverter is obtained by controlling the semiconductor switches ON and OFF to generate the desired output. Pulse width modulation (PWM) techniques are widely used to perform this task. In the simplest form, three reference signals are compared to a high frequency carrier waveform. The result of that comparison in each leg is used to turn the switches ON or OFF. This technique is referred to as sinusoidal pulse width modulation (SPWM). It should be noted that the switches in each leg should be operated interchangeably, in order not to cause a short circuit of the DC supply.

Insulated Gate Bipolar Transistors (IGBTs) and power MOSFET devices can be used to implement the switches. Each device varies in its power ratings and switching speed. IGBTs are well suited for applications that require medium power and switching frequency **[11]**.

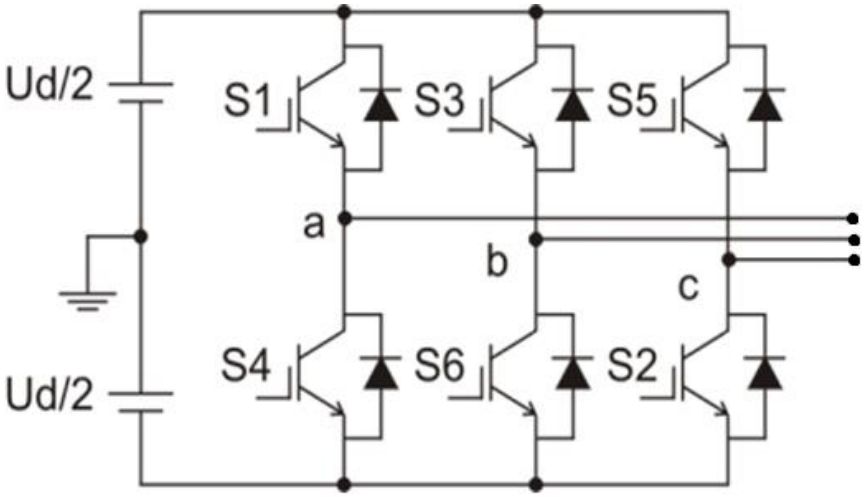


Figure 2.1. Three-Phase Bridge Inverter circuit.

### 2.1.2. Sinusoidal PWM

The sinusoidal pulse-width modulation (SPWM) technique produces a sinusoidal waveform by filtering an output pulse waveform with varying width. A high switching frequency leads to a better filtered sinusoidal output waveform. The desired output voltage is achieved by varying the frequency and amplitude of a reference or modulating voltage. The variations in the amplitude and frequency of the reference voltage change the pulse-width patterns of the output voltage but keep the sinusoidal modulation.

As shown in figure 2.2, a low-frequency sinusoidal modulating waveform is compared with a high-frequency triangular waveform, which is called the carrier waveform. The switching state is changed when the sine waveform intersects the triangular waveform. The crossing positions determine the variable switching times between states.

In three-phase SPWM, a triangular voltage waveform ($V_T$) is compared with three sinusoidal control voltages ($V_a$, $V_b$, and $V_c$), which are 120° out of phase with each other and the relative levels of the waveforms are used to control the switching of the devices in each phase leg of the inverter.

A six-step inverter is composed of six switches $S_1$ through $S_6$ with each phase output connected to the middle of each inverter leg as shown in figure 2.1. The output of the comparators in figure 2.2 form the control signals for the three legs of the inverter. Two switches in each phase make up one leg and open and close in a complementary fashion. That is, when one switch is open, the other is closed and vice-versa. The output pole voltages $V_{ao}$,

$V_{bo}$, and $V_{co}$ of the inverter switch between $-V_{dc}/2$ and $+V_{dc}/2$ voltage levels where $V_{dc}$ is the total DC voltage.

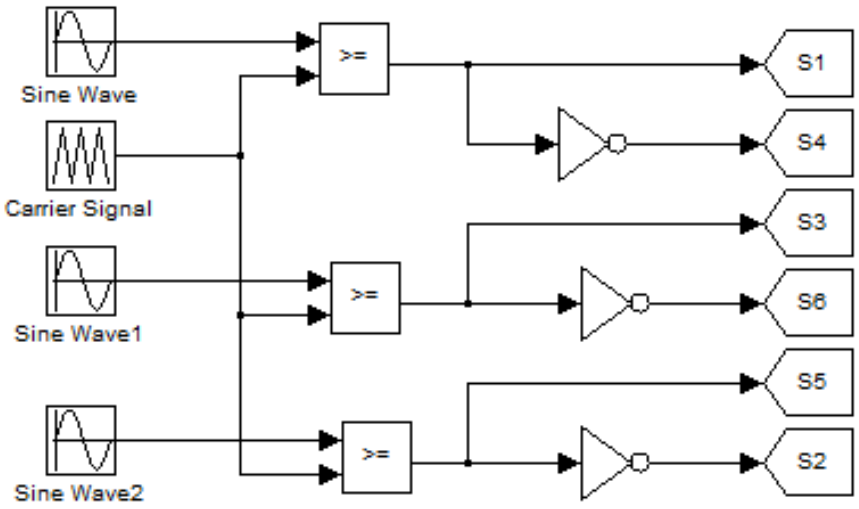


Figure 2.2. Control Signal Generator for SPWM.

The peak of the sine modulating waveform is always less than the peak of the triangle carrier voltage waveform. When the sinusoidal waveform is greater than the triangular waveform, the upper switch is turned on and the lower switch is turned off. Similarly, when the sinusoidal waveform is less than the triangular waveform, the upper switch is off and the lower switch is on. Depending on the switching states, either the positive or negative half DC bus voltage is applied to each phase. The switches are controlled in pairs ((S1, S4), (S3, S6), and (S5, S2)) and the logic for the switch control signals is:

- $S_1$ is ON when $V_a > V_T$ $S_4$ is ON when $V_a < V_T$
- $S_3$ is ON when $V_b > V_T$ $S_6$ is ON when $V_b < V_T$
- $S_5$ is ON when $V_c > V_T$ $S_2$ is ON when $V_c < V_T$.

As seen in figure 2.3, the pulse widths depend on the intersection of the triangular and sinusoidal waveforms. The inverter output voltages are determined as follows:

If $V_a > V_T$ then $V_{ao} = 0.5V_{dc}$

$V_b > V_T$ then $V_{bo} = 0.5V_{dc}$

$V_c > V_T$ then $V_{co} = 0.5V_{dc}$

And if $V_a < V_T$ then $V_{ao} = -0.5V_{dc}$

$V_b < V_T$ then $V_{ao} = -0.5V_{dc}$

$V_c < V_T$ then $V_{ao} = -0.5V_{dc}$

The inverter line-to-line voltages are obtained from the pole voltages as:

$$V_{ab} = V_{ao} - V_{bo}$$

$$V_{bc} = V_{bo} - V_{co}$$

$$V_{ca} = V_{co} - V_{ao}$$

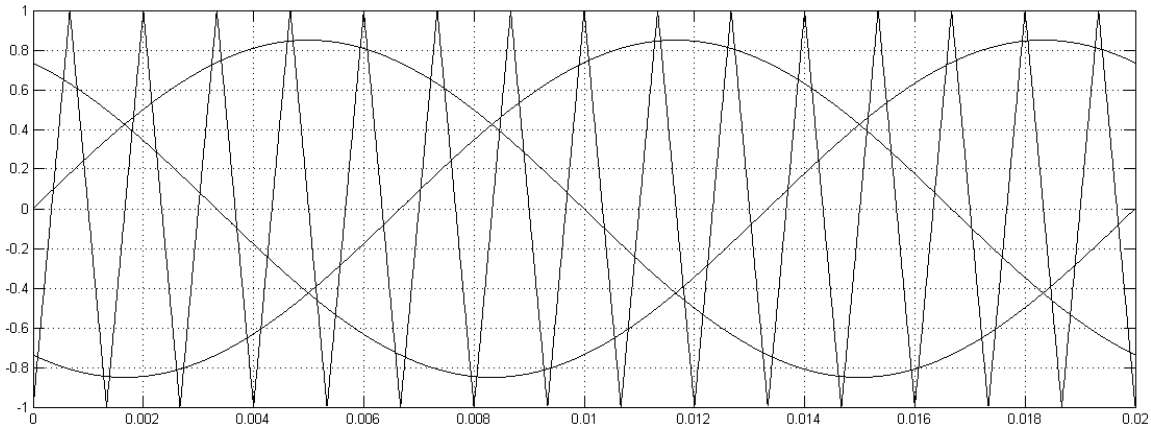

Figure 2.3. Carrier and modulating Signals for 2-Level Inverter

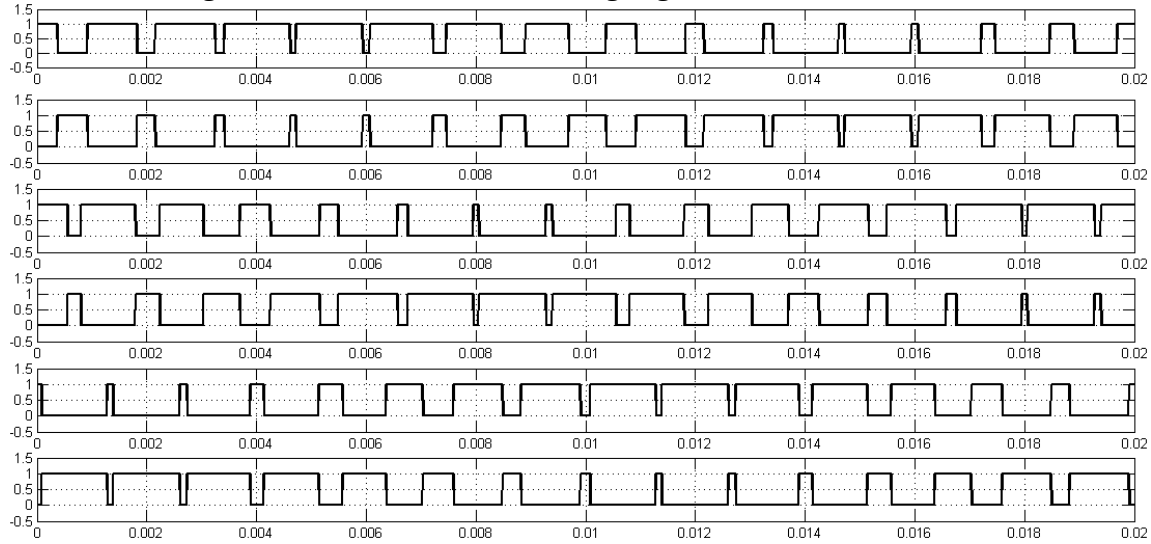

Figure 2.4. Firing Pulses to Six MOSFETS S1, S4, S3, S6, S5, S2 from Top to Bottom.

## 2.2. Three level Three Phase Diode Clamped Multilevel Inverter

### 2.2.1. Inverter Circuit

Diode clamped inverter is the most commonly used multilevel topology in which the diode is used as the clamping device to clamp the dc bus voltage in order to achieve steps in

the output voltage. In general the voltage across each capacitor for an m-level diode clamped inverter at steady state is $V_{dc}/(m-1)$. The diode-clamped inverter provides multiple voltage levels through connection of the phases to a series of capacitors. In three-level inverter, two capacitors are connected across the dc bus resulting in one additional level. The additional level is the neutral point of the DC bus.

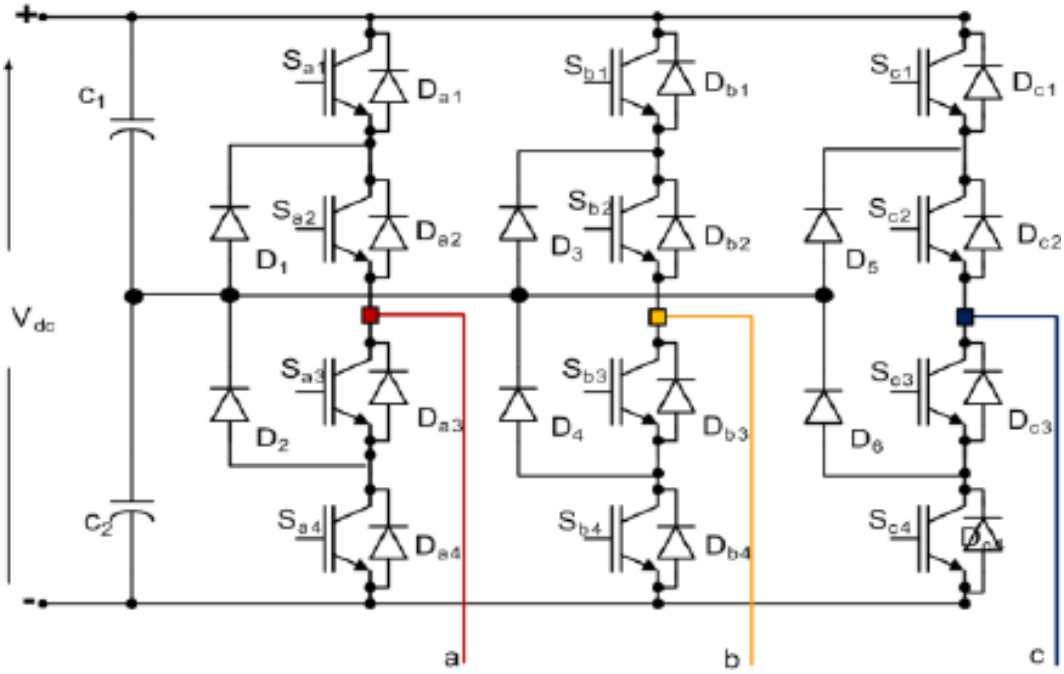


Figure 2.5. Three-phase three-level DCMLI.

A three-phase three-level diode-clamped inverter is shown in Fig. 2.5. In this circuit, the DC bus voltage is split in to three levels by two series connected bulk capacitors $C_1$ and $C_2$. The middle point of the two capacitors 'n' can be defined as the neutral point. The diodes $D_1$ and $D_1$ clamp the switch voltage to half the level of the DC bus voltage.

The key component that decide this circuit from a conventional two level converter is $D_1$ and $D_2$. These two diodes clamp the switch voltage to half the level of the dc bus voltage. When both $S_{a1}$ and $S_{a2}$ are on, the voltage across $V_{a0}$ is $V_{dc}$. In this case, $D_2$ balances the voltage sharing between $S_{a3}$ and $S_{a4}$ with $S_{a3}$ blocking the voltage across $C_1$ and $S_{a4}$ blocking the voltage across $C_2$. The circuit has three output voltage levels: $V_{dc}$, $V_{dc/2}$, and 0. The phase output voltage has three states: $V_{dc/2}$, 0 and $V\text{-}_{dc/2}$. DCMLI has the following advantages.

**Advantages:**

- DC-link capacitors are common to three phases.
- Switching frequency can be low.
- Reactive current and negative-phase-sequence current can be controlled.

### 2.2.2. Level Shifted PWM

A level shifted sinusoidal PWM technique is used to control the three level DCMLI. Fig. 2.6 shows the control signal generation diagram for a 3-level Diode-clamped inverter. In 3-level inverter two triangular carrier signals are compared with three sinusoidal modulating signals as shown in Fig. 2.6. The two carrier signals are shifted in their magnitude (Level-Shifted PWM). The three sinusoidal signals are phase displace by 120$^{o}$. The three signals developed in the simulation for the control signals generation of a phase are shown in Fig. 2.7. Firing pulses are generated according to the logic given in previous chapter. The Fig. 2.8 shows the firing pulses for the four MOSFETs in one phase leg of 3-level Diode-clamped inverter.

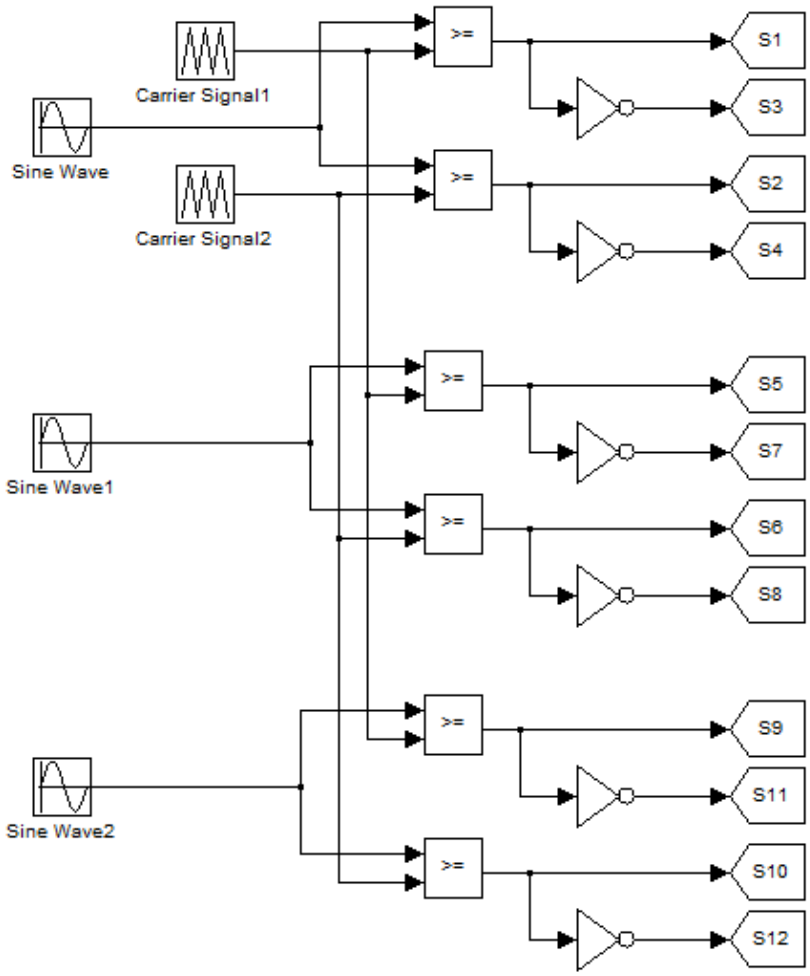


Figure 2.6. Control Signal Generation for 3-Level Diode-Clamped Inverter

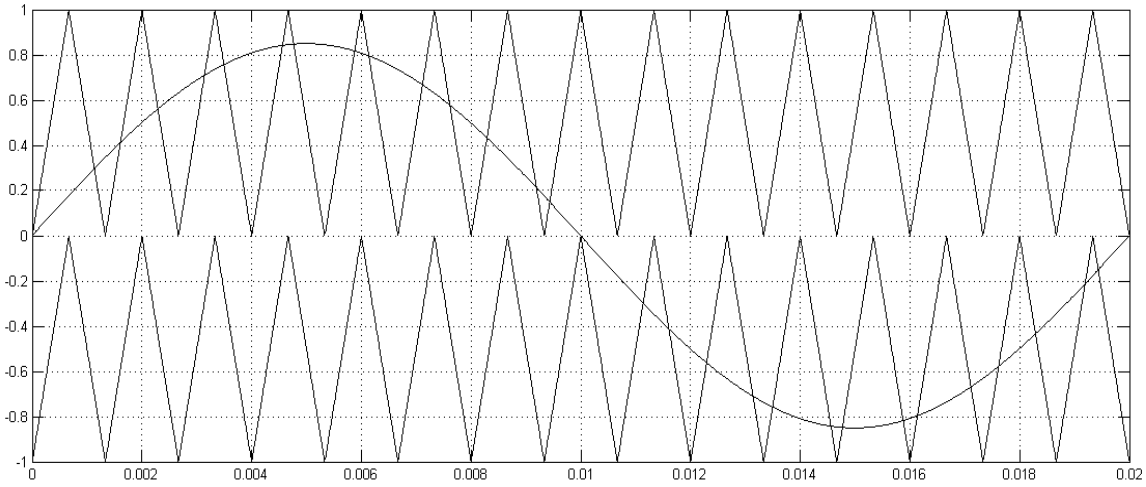


Figure 2.7. Carrier and modulating Signal for one Phase Leg of 3-Level Diode-Clamped Inverter

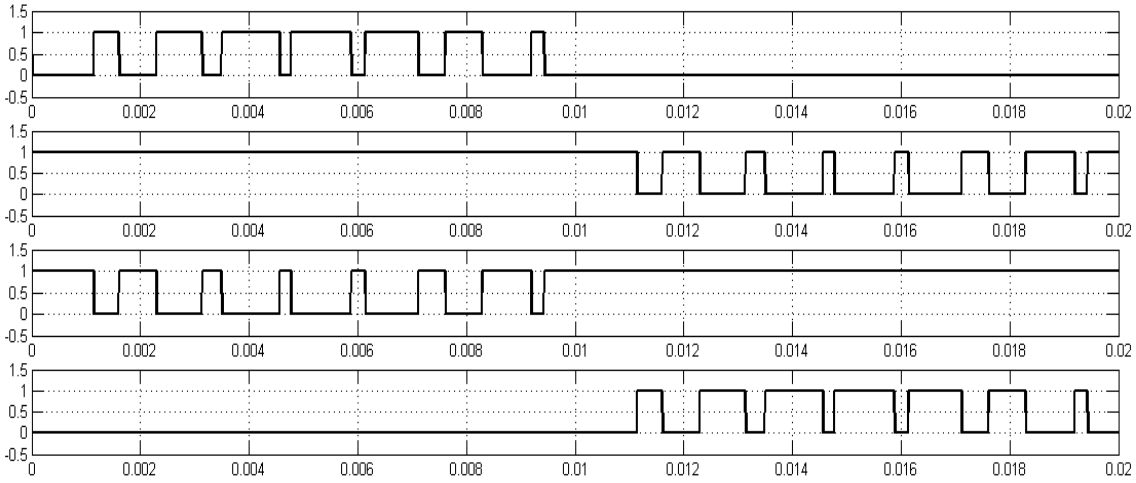


Figure 2.8. Firing Pulses to Four MOSFETS of a Phase Leg of 3-Level Diode-Clamped Inverter

# Chapter 3: PHOTOVOLTAIC SYSTEM

Exhaustive description of various components of the grid connected PV system is presented in this chapter, including the control structures involved, except for generation of control pulses for the PV inverters, which has been clearly explained in chapter 2.

***Solar energy***

Solar energy is considered to be one of the most promising and reliable sources of renewable energy. It features following significant advantages over conventional energy resources: it is pollution-free, no moving parts involved in operation, durable and less maintenance. Solar energy source, the sun is inexhaustible and free of cost.

Available non-conventional sources of energy on earth are solar radiation, secondary solar-powered resources comprising of wave and wind power, biomass and hydroelectricity. Solar energy is mostly used in the generation of electricity, heating and cooking.

Solar Photovoltaic arrays converts sunlight into electricity directly. Harnessing of solar energy is only possible during daylight. It acts as safe, clean and strategically sounding alternative to current techniques of generation of electricity. Solar photovoltaic system is an attractive option considering existing high residential tariffs, abundance of solar radiation source, and the cost reduction trend of solar modules [6].

***Components of grid connected system***

Several components are needed to construct a grid connected PV system to perform the power generation and conversion functions. In figure 3.1**,** block diagram of grid connected PV system using Voltage Source Inverter (VSI) is shown. A PV array is used to convert the light from the sun into DC current and voltage. A DC converter is connected to the PV array to increase its terminal voltage and provide the means to implement an MPPT technique by controlling its switching duty cycle. The output power from the array is stored temporarily in large capacitors to hold power before DC/AC power conversion. A three phase inverter is then connected to perform the power conversion of the array output power into AC power suitable for injection into the grid. Pulse width modulation control is one of the

techniques used to shape the magnitude and phase of the inverter output voltage. Three phase VSI structure has been analyzed in chapter 2.

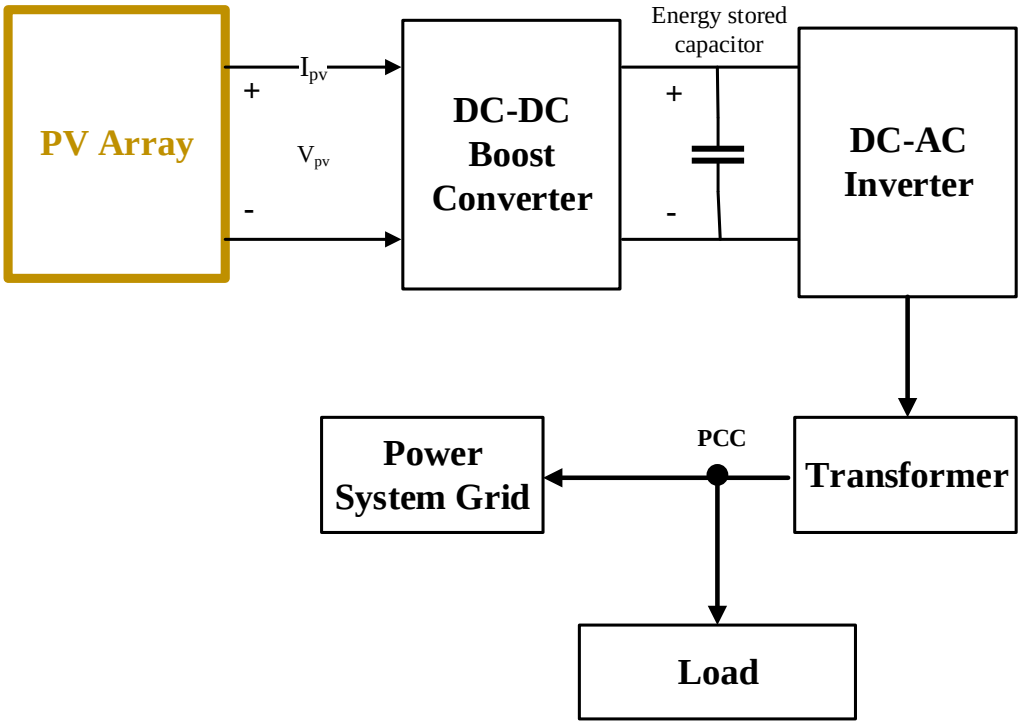


Figure 3.1. General structure of a grid-connected PV system using VSI.

## 3.1. Modelling of Photovoltaic (PV) module

A Photovoltaic (PV) module is a collection of a number of solar cells connected in both the series and parallel fashion. When connected in series, module voltage increases, while current increases when strings of PV cells are connected in parallel. Modelling of a single solar cell is done by using a current source, a diode and two resistors. The resulting model is known as single diode model of solar cell. The corresponding single diode model (see Figure 3.2) consists of a diode for cell polarization and the two resistors, namely, series and shunt for the losses involved. [7]

The PV cell is essentially a non-linear DC current source. It supplies variable power which depends on variation of the temperature along with irradiation. Either of the Thevenin' or the Norton' circuit can be used for the equivalent circuit of PV cells. [7]

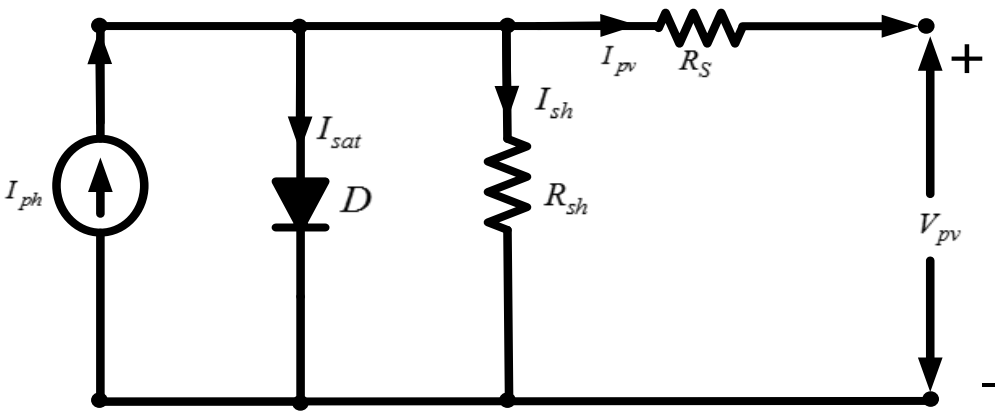


Figure 3.2. Equivalent circuit of PV module

V-I relations of this model is given by the following equations

$$I = N_p I_{ph} - N_p I_{sat}(e^{(\frac{qv}{KTAN_s})} - 1) \tag{3.1}$$

$$I_{sat} = I_{rr}\left[\frac{T}{T_r}\right]^3 e^{(\frac{qE_g}{KA}[\frac{1}{T_r}-\frac{1}{T}])} \tag{3.2}$$

$$P = VI = N_p I_{ph} V - N_p I_{sat} V[e^{(\frac{qv}{KTAN_s})} - 1] \tag{3.3}$$

Where

$I$ = output current of PV Module, $V$ = output voltage of PV Module, $I_{ph}$ = light induced current of single PV cell, $I_{sat}$ = diode saturation current of single PV cell, $N_p$ = no. of PV cell in parallel, $N_s$ = no. of PV cell in series, $q$ = elementary charge ($1.602\times10^{-19}C$), $K$ = Boltzmann constant $(1.38\times10^{-23} j/^0 \text{K})$, $T$ = surface Temperature of PV Module $(^0K)$, $T_r$ = reference cell temperature $(^0K)$, $A$ = diode ideality factor, $I_{scr}$ = cell short-circuit current at reference temperature, $I_{sat}$ = saturation current of the cell, $E_g$ = band gap energy of the semiconductor used in cell, $S$ = solar radiation and $k_i$ = short-circuit current temperature coefficient

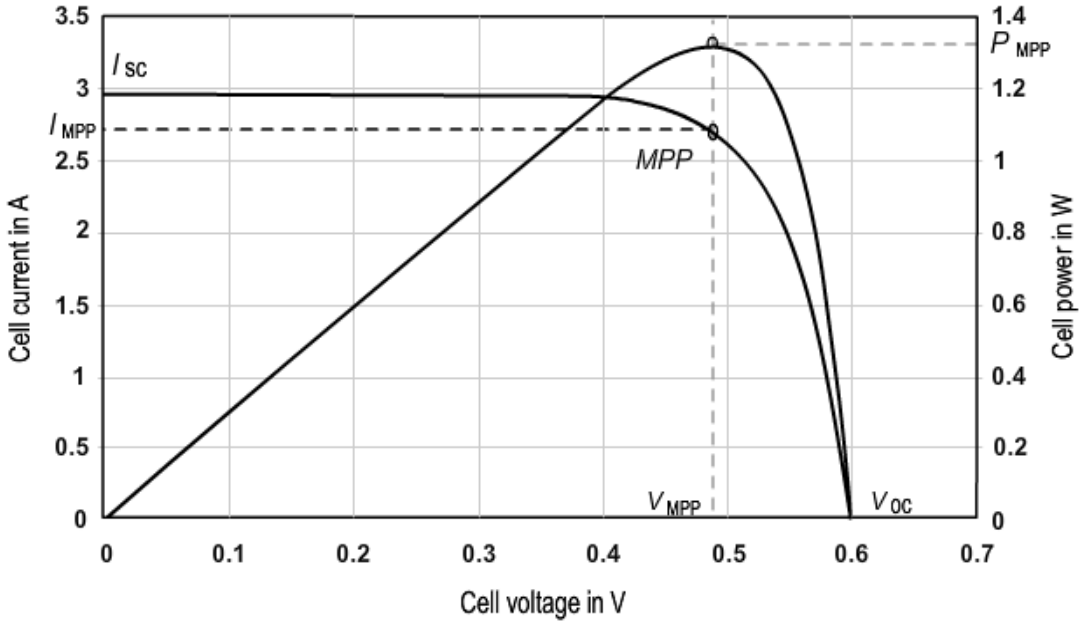


Figure 3.3. P-V, I-V characteristic of PV array.

Based on the eqn. (3.1) and eq. (3.3) I-V and P-V characteristics are sketched are shown in Figure 3.3. The maximum output power is denoted by $P_{MPP}$, voltage by $V_{MPP}$ and current by $I_{MPP}$. In these curves, three points are noticeable:

**Short circuit point,** in which the voltage over the module is zero, but the current is at the maximum (= short circuit current $I_{SC}$).

**Maximum Power Point (MPP),** where the product of current and voltage has its maximum $(I_{MPP} \times V_{MPP})$.

**Open circuit point,** where the current is zero and the voltage is at its maximum. (Open circuit voltage $V_{oc}$).

***Effect of variation of solar irradiation***

The P-V and I-V characteristics of solar cell are very dependent on the solar irradiation values as indicated in eqn**. (**3.1)-(3.3). Solar irradiation has a tendency of fluctuating with environmental changes. Thus, there are control mechanisms available that can track this change and can modify the functioning of the solar cell to assist the resulting load demands. Higher the solar irradiation higher will be the solar input influx to the solar cell due to which power magnitude is highly likely to increase to match value of voltage.

With the increase in solar irradiance, the open circuit voltage increases. Consequently, more power is generated. Figure 3.4 and 3.5 respectively present the variation of P-V curves and I-V curves at different irradiation values.

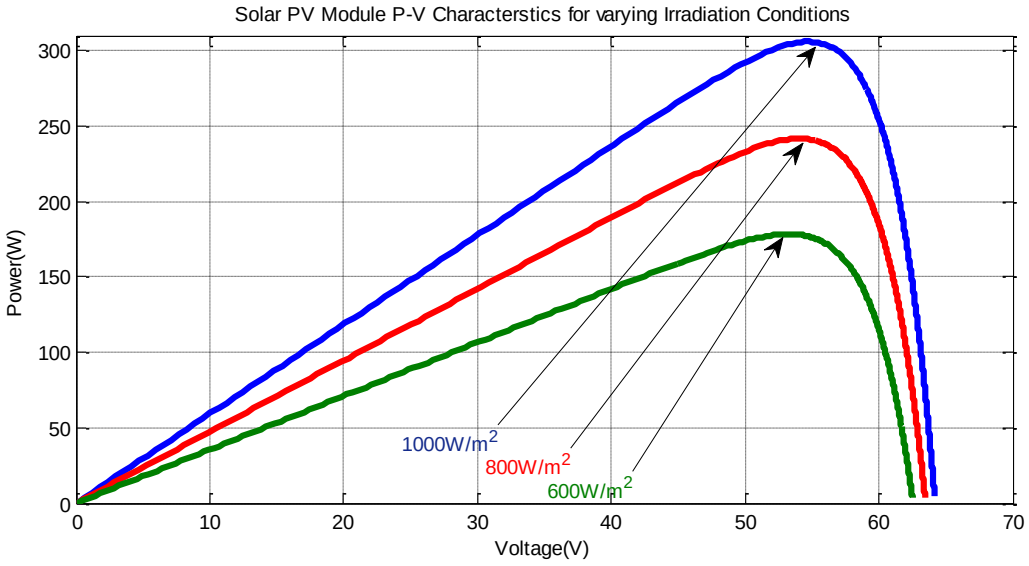


Figure 3.4. Solar P-V curves at different irradiation values

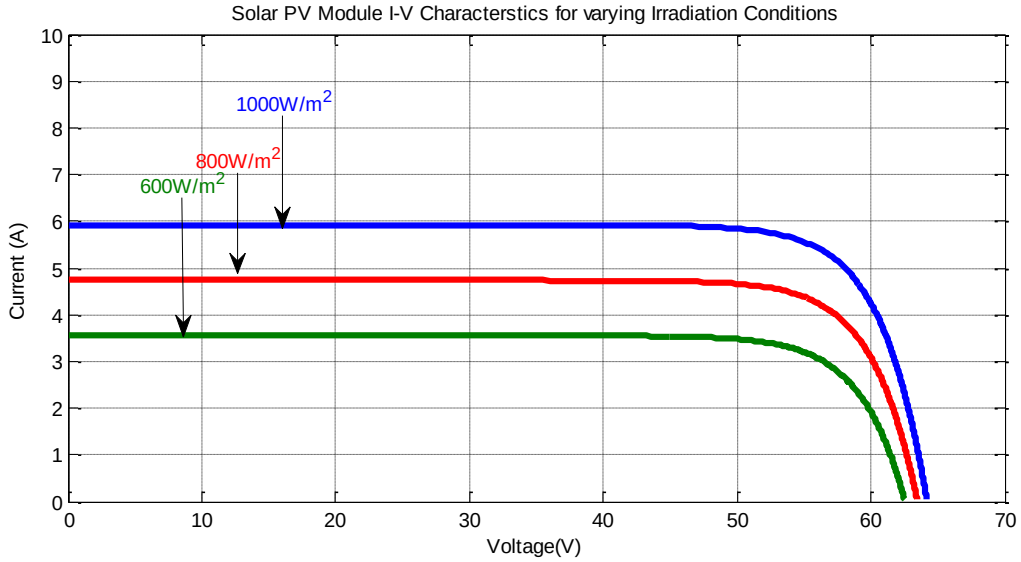


Figure 3.5. Solar I-V curves at different irradiation values

***Effect of variation of temperature***

With the variation in temperature, functioning of the power generation capacity is affected due to the resulting fluctuation. A decrease in the value of the open circuit voltage is followed by an increase in temperature. Any increase in temperature amplifies the band

gap of the concerned material, so more energy becomes essential to cross the existing potential barrier. As a consequence, the efficiency of the solar cell decreases [7]. The variation of P-V curves and I-V curves at different temperature is shown in Figure 3.6 and 3.7 respectively.

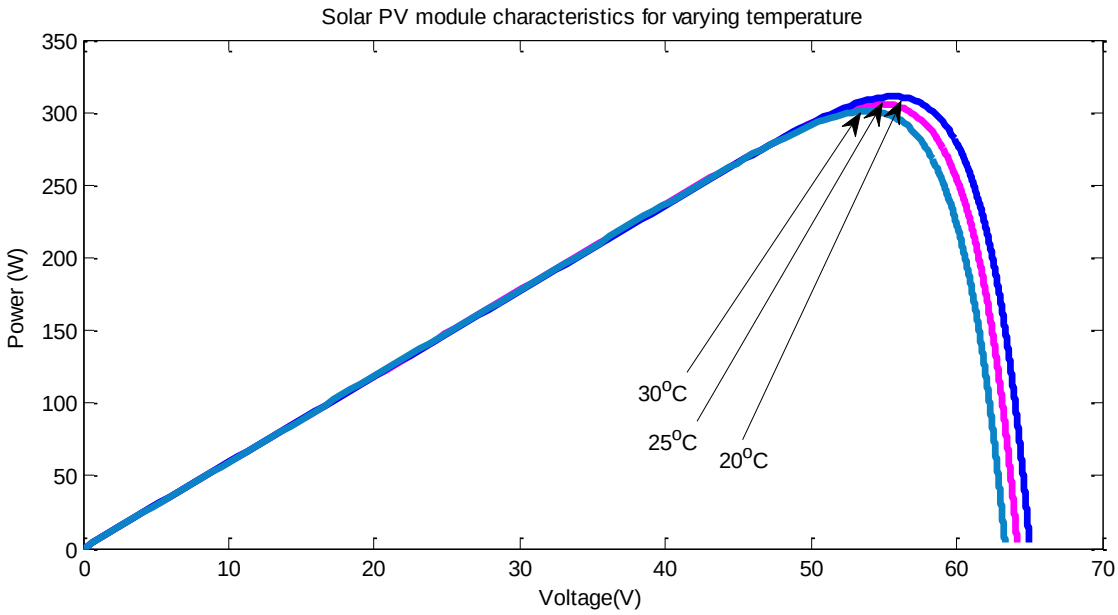


Figure 3.6. Variation of Power vs. Voltage with respect to change in temperature

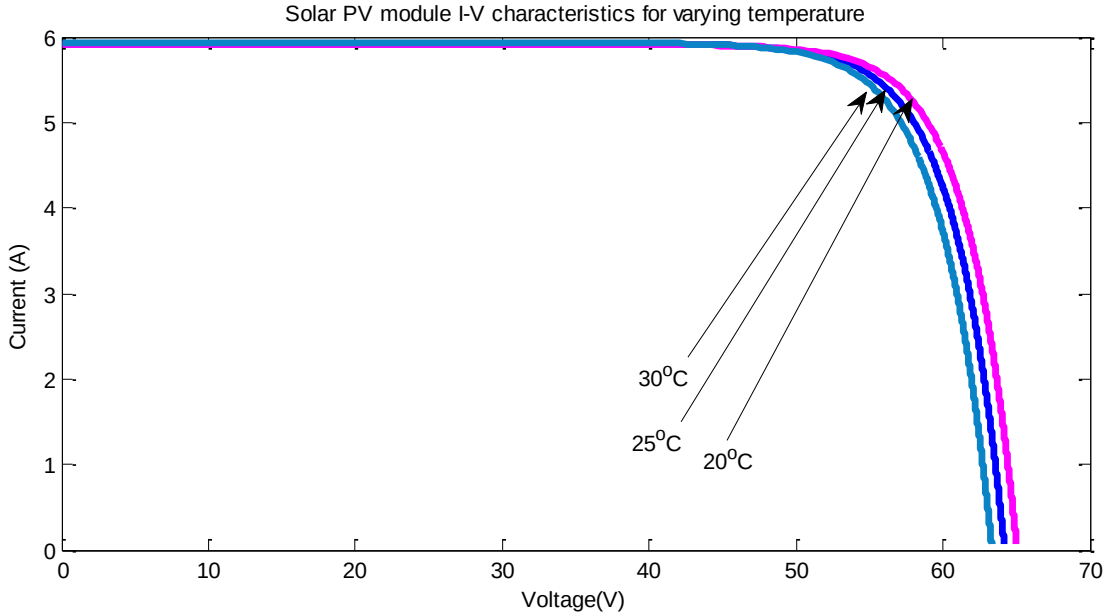


Figure 3.7. Variation of Current vs. Voltage with respect to change in temperature

A photovoltaic (PV) array has nonlinear I-V (current-voltage) characteristics and its output power varies with solar irradiance level, besides the ambient temperature. Only one point, called maximum power point (MPP), exists on the P–V (power–voltage) curve, in which the power is maximum. MPP fluctuates with the changes in atmospheric conditions. In the same way, energy conversion efficiency of the PV module becomes very low and the resulting discrepancy between the source and the load characteristics creates significant power losses. Consequently, the maximization of power output that takes place with greater efficiency becomes substantial. MPPT is the technique that is used for extracting maximum power which is made available from the PV module [8].

## 3.2. Incremental Conductance MPPT Technique

Under a given weather condition MPPT techniques are employed in control DC-DC converters in order to extract maximum output power from a PV array. The DC-DC converter is controlled continuously to operate the array at its maximum power point in spite of possible changes in the load impedance. Different techniques have been established to provide maximum power tracking of PV arrays. Some of the techniques are:

- Constant Voltage (CV)
- Open Voltage (OV)
- Short-Current Pulse Method (SC)
- Perturb and Observe Methods (P & O )
- Incremental Conductance Method(IC);
- Artificial Neural Network method,
- Fuzzy Logic method [8].

Comparison of performances of these techniques are performed on certain desirable features such as hardware implementation, cost, complexity, speed, sensors required, range of effectiveness, steady state error, dynamic response, efficiency of the system and stability. From the literature reviewed, it can be safely concluded that P&O and Incremental conductance methods are used widely owing to their advantages. Due to sudden change in atmospheric conditions tracking in wrong direction cannot be prevented [9]. Though, P&O technique faces a problem of oscillation around MPP, because of which significant power loss takes place. Oscillation of P&O system around the MPP resulting in loss of PV power due to continuous disturbances to seek the MPP [9]. Incremental Conductance power tracking

is implemented in this project as it is comparatively better amongst all conventional techniques.

This algorithm make use of the fact that the slope of the P-V curve of a PV array is equal to zero at the maximum power point (MPP), as shown in figure 3.3. The slope is positive in the area to the left of the maximum power point and negative in the area to the right. This can be simplified using the following approximation:

$$\frac{dP}{dV} = \frac{d(IV)}{dV} = I + V\frac{dI}{dV} = I + V\frac{\Delta I}{\Delta V}$$

From this:

At MPP,

$$\frac{\Delta I}{\Delta V} = -\frac{I}{V}$$

At left of MPP,

$$\frac{\Delta I}{\Delta V} > -\frac{I}{V}$$

At right of MPP,

$$\frac{\Delta I}{\Delta V} < -\frac{I}{V}$$

The incremental conductance algorithm is illustrated in figure 3.8, where $V_{ref}$ is used as a reference control signal for the DC converter [10].

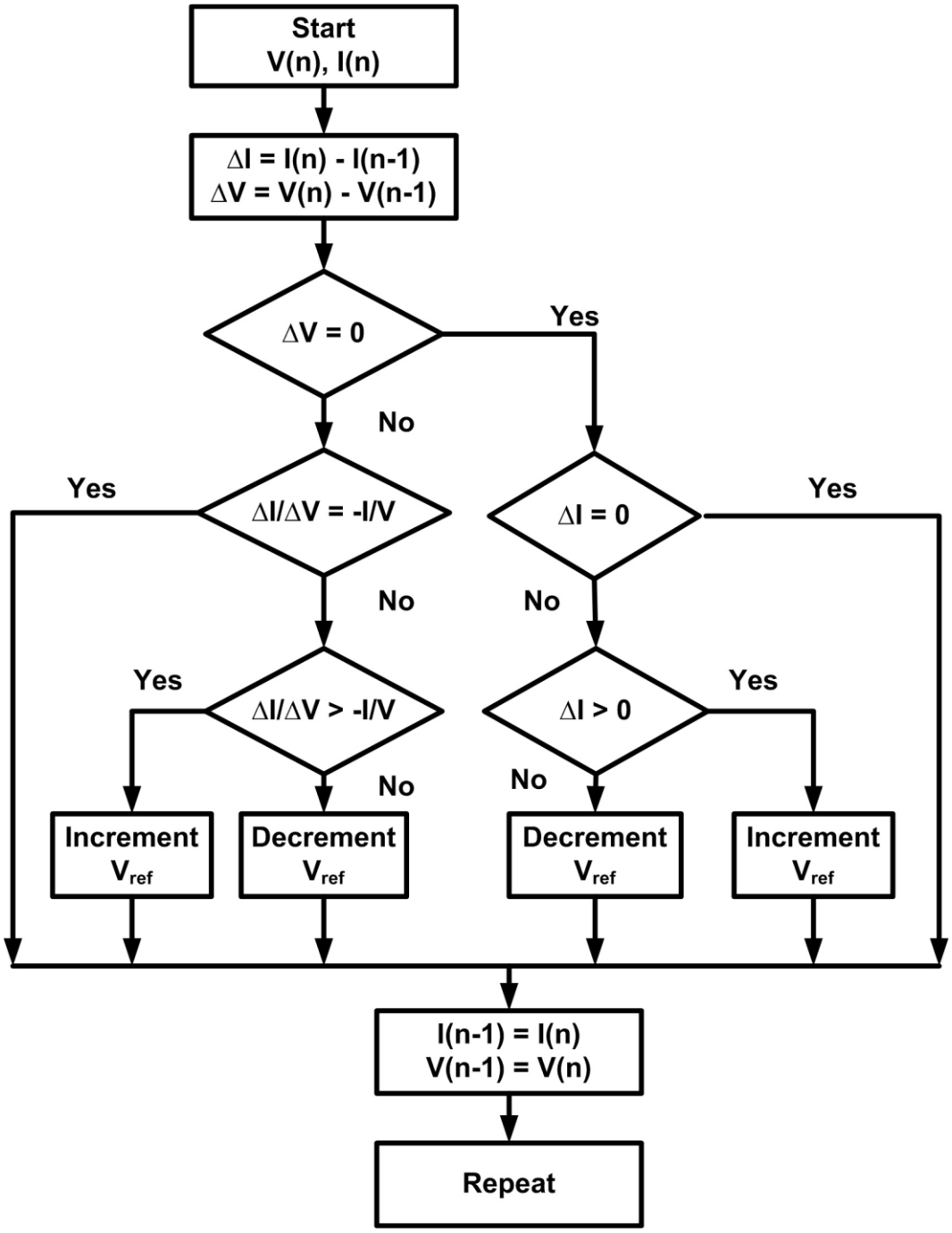


Figure 3.8. Flowchart depicting Incremental conductance algorithm

As comparison of different MPPT techniques INC complexity is medium, tracking accuracy is good under varying atmospheric conditions and tracking factor is good.

## 3.3. DC-DC Converter (Boost Converter)

The choice of right converter has an important effect in the optimum performance of the photovoltaic system. A simple DC-DC converter converts fixed DC voltage into variable DC voltage.

Non-isolated topologies of DC-DC converters are categorized into three types: Step down (Buck), Step up (Boost), and Step up and down (Buck-Boost). The buck topology is used for voltage step-down. The buck type converter is usually used in PV applications for charging batteries. Further, boost type converter is used in grid connected systems for stepping up the output voltage to the utility level before DC-AC conversion stage.

Boost converters have numerous advantages over buck converters, two of them are better dynamic response and cheaper implementation. Buck converter requires a huge thus expensive capacitor for the smoothening of the uneven output current of the PV module. The current rating is lower in boost topology in case of power MOSFETs and drivers as well. Further, boost converter requires a low-side MOSFET driver, and such a driver is simple and cheap in comparison with the high-side driver of buck converter. When blocking diodes are considered, boost topology reproduces substantial advantages over buck topology. The free-wheeling diode can act as the blocking diode dodging reverse current in boost topology. The blocking diode in buck converter is an extra component conducting the complete output current.

Input voltage magnitude is step up by boost converter to a required output voltage magnitude when not using a transformer. Essential components of a boost converter are inductor, a diode, and a high frequency switch. The three components provide power to the load at a voltage higher than the input voltage in an effective manner. This control strategy is based on the manipulation of the duty cycle of the switch causing the voltage change

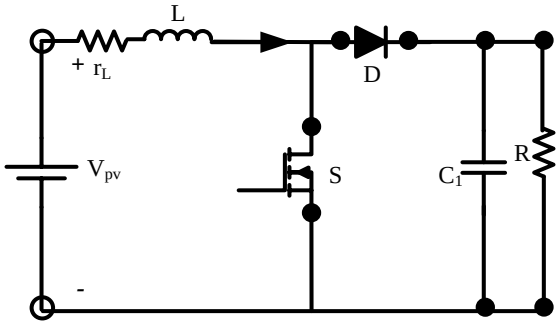


Figure 3.9. Boost Converter

Boost converter operates in two modes. The operation is based on the closing and opening of the switch. In the first mode, the switch is closed; this is known as the charging mode of operation. The second mode, discharging mode is when the switch is open [11].

***Charging Mode***

In this mode of operation; the switch is closed and the inductor is charged by the source. The charging current is exponential in nature but for simplicity it is assumed to be linearly varying. Flow of current from the source to the load is restricted by the diode and the demand of the load is met by the discharging of the capacitor. The charging time is denoted by $T_{on}$. Figure 3.10 shows the equivalent circuit.

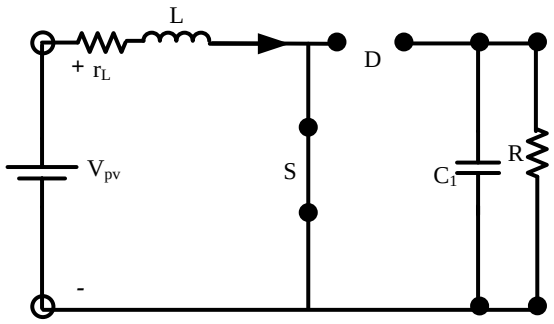


Figure 3.10. Equivalent circuit of boost converter when switch is closed

***Discharging Mode***

In this mode of operation, the switch is open and the diode is forward biased. The inductor discharges and together with the source charges the capacitor to meet the load requirements. The variation in load current is very small and in many cases is assumed constant throughout the operation. Figure 3.11 shows the equivalent circuit.

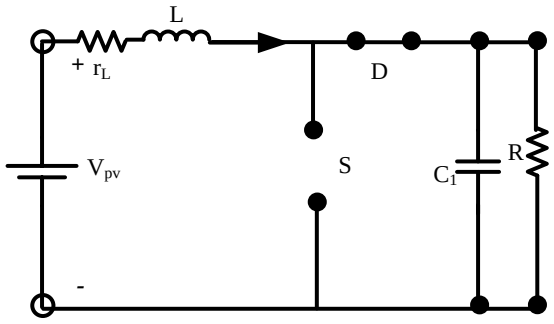


Figure 3.11. Equivalent circuit of boost converter when switch is open

***Steady state analysis of boost converter***

In charging mode the eqn. becomes $(0 < t_1 < DT)$

$$V_{in} = L\frac{dI}{dt_1} \tag{3.4}$$

In discharging mode the eqn .becomes $(DT < t_2 < (1-D)T)$

$$V_{in} - V_{out} = L\frac{dI}{dt_2} \tag{3.5}$$

Let $t_1 = DT$ and $t_2 = (1-D)$

Comparing eqn. (3.9) and eqn. (3.10) we get

$$\frac{V_{out}}{V_{in}} = \frac{1}{1-D} \tag{3.6}$$

Where $D = \frac{T_{on}}{T}$ and $T = \frac{1}{f}$

***Inductor Selection***

Choosing inductor is one of the most vital task in designing a DC/DC converter. Higher value of maximum possible output current results in higher value of the inductor. We can use the following for inductance value:

$$L = \frac{V_{in} * (V_{out} - V_{in})}{\Delta I_L * f_s * V_{out}}$$

Where, $V_{in}$ is the typical input voltage, $f_s$ is the minimum switching frequency of the converter, and $\Delta I_L$ is the estimated inductor ripple current as discussed below.

A smaller ripple reduces the magnetic hysteresis losses in the inductor, as well as output voltage ripple and EMI. But in the same way, regulation time rises at load changes. In addition, a larger inductor increases the total system costs. A good estimation for the inductor ripple current is 20 % to 40 % of the output current. Inductor Ripple Current can be found out as below:

$$\Delta I_L = (0.2 \; to \; 0.4) * I_{out\,(\max)} * \frac{V_{out}}{V_{in}}$$

Where, $I_{out\,(\max)}$ is the maximum output current desired in the application.

***Output Capacitor Selection***

For calculation of minimum output capacitance value, following formula is used:

$$C_{out(\min)} = \frac{I_{out(\max)} * D}{f_s * \Delta V_{out}}$$

Where, $C_{out(\min)}$ is the minimum output capacitance, $I_{out\,(\max)}$ is the maximum output current desired in the application, and $f_s$ is the minimum switching frequency of the converter.

The output of dc-dc boost converter need to be converted to ac to feed ac loads or grid. The inverter is expected to possess capability of inversion of electrical power with less harmonic content (lesser than IEEE 1547 standards) along with active and reactive power controlling capabilities.

## 3.4. Three phase inverter (DC-AC converters)

Three phase inverters are used to convert output dc voltage of boost converter to AC voltages, thus acting as DC-AC interface. In this work, PV grid connected system using three topologies of such inverters is realized, namely, three leg Bridge Inverter (2-level), three leg Diode Clamped Multilevel Inverter (DCMLI, 3-level), and, Cascaded Multilevel Inverter (CCMLI, 3-level). These topologies have been introduced in Chapter 2 of this work. The inverters will normally operate in dynamic VAR compensation mode for voltage support including low PV and no PV periods [12].

### 3.4.1. System Structure

Grid interconnection of PV system is achieved through the inverter, which converts generated dc power from PV modules to ac power used for powering the electric equipment.

The output of the PV array is connected to a boost DC-DC converter that is used to perform MPPT functions and step up the array terminal voltage. A controller for DC converter is used to perform these two functions. A DC link capacitor is used at the output of DC-DC converter which acts as a temporary power storage device to achieve steady power

flow through VSI. The regulation of capacitor's voltage is done using a DC link controller that balances input and output powers of the capacitor.

The voltage source inverter is controlled in the rotating *dq* frame for injecting a controllable three phase AC current into the grid. Current is injected in phase with the grid voltage to achieve unity power factor operation. A phase locked loop (PLL) is used to lock on the grid frequency and provide a stable reference synchronization signal for the inverter control system, so as to minimize the error between the actual injected current and the reference current obtained from the DC link controller. An inductor is placed for coupling purpose between inverter and PCC, providing a smooth output current which is low in harmonic content.

### 3.4.2. The *abc* / *dq* Transformation

The *dq* transformation is used to transform three phase system quantities like voltages and currents from the synchronous reference frame (*abc*) to a synchronously rotating reference frame with three constant components when the system is balanced. The relationship that govern the transformation from the *abc* to *dq* frame is

$$\begin{bmatrix} x_d \\ x_q \\ x_0 \end{bmatrix} = T \times \begin{bmatrix} x_a \\ x_b \\ x_c \end{bmatrix}$$

$$T = \sqrt{\frac{2}{3}} \times \begin{bmatrix} \cos(\omega t) & \cos(\omega t - 2\pi/3) & \cos(\omega t + 2\pi/3) \\ -\sin(\omega t) & -\sin(\omega t - 2\pi/3) & -\sin(\omega t + 2\pi/3) \\ 1/\sqrt{2} & 1/\sqrt{2} & 1/\sqrt{2} \end{bmatrix}$$

where *x* can be either a set of three phase voltages or currents to be transformed, *T* is the transformation matrix and $\omega$ is the angular rotation frequency of the frame [13]. The angle between the direct axis (d-axis) and phase a-axis is defined as θ as shown in figure 3.11.

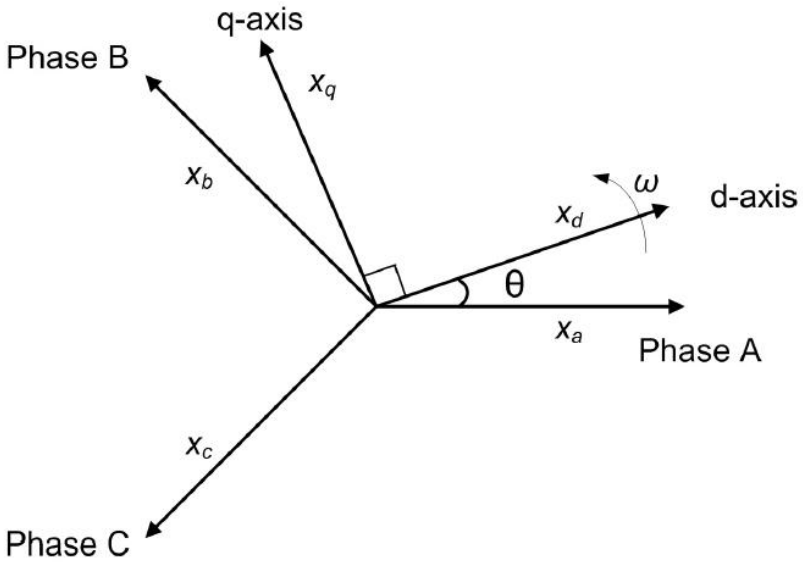


The result of this transformation is three constant rotating components: the direct (d), quadrature (q) and zero (0) components. In balanced three phase systems, the zero component can be ignored since

$$x_a + x_b + x_c = 0$$

The inverse transformation from the *dq* frame to the *abc* frame can be obtained by applying

$$\begin{bmatrix} x_a \\ x_b \\ x_c \end{bmatrix} = T^{-1} \times \begin{bmatrix} x_d \\ x_q \\ x_0 \end{bmatrix}$$

$$T^{-1} = \sqrt{\frac{2}{3}} \times \begin{bmatrix} \cos(\omega t) & -\sin(\omega t) & 1/\sqrt{2} \\ \cos(\omega t - 2\pi/3) & -\sin(\omega t - 2\pi/3) & 1/\sqrt{2} \\ \cos(\omega t + 2\pi/3) & -\sin(\omega t + 2\pi/3) & 1/\sqrt{2} \end{bmatrix}$$

This transformation is useful in developing the control system for the voltage source inverter under current control to regulate the output of the PV system. Active and reactive powers injected from the PV system can be calculated using the following relationships

$$P = V_d I_{d,injected} + V_q I_{q,injected}$$

$$Q = -V_d I_{q,injected} + V_q I_{d,injected}$$

where $V_d$, $V_q$ are the *dq* voltages at PCC (Point of Common Coupling) at the grid side of the transformer, $I_{d,injected}$ and $I_{q,injected}$ are the *dq* components of the injected current at the grid side. It is evident that in the computation of reactive power *Q*, there is cross coupling between the direct and quadrature current and voltage components. This can be eliminated through the use of a phase locked loop (PLL) that locks on the grid frequency in such a way that the quadrature component of the voltage at the point of PV system connection is forced to zero. So, *P* and *Q* becomes,

$$P = V_d I_{d,injected}$$

$$Q = -V_d I_{q,injected}$$

This means that the direct and quadrature components of the inverter output current can be used to control the active and reactive output powers from the PV array system, as they are related to the injected currents by the transformer turns ratio. This is based on the assumption that the voltage at the point of common coupling (PCC) is relatively constant. In current practice, distribution systems have regulation mechanisms to keep voltage within specified limits.

### 3.4.3. Phase Locked Loop (PLL)

The role of the phase locked loop is to provide the rotation frequency, direct and quadrature voltage components at the point of common coupling (PCC) by resolving the grid voltage *abc* components. Multiple control blocks of the PV system rely on this information to regulate their output command signals. As stated earlier, the PLL computes the rotation frequency of the grid voltage vector by first transforming it to the *dq* frame, and then force the quadrature component of the voltage to zero to eliminate cross coupling in the active and reactive power terms [13]. A proportional-integral controller is used to perform this task as shown in figure 3.12. The proportional ($K_p$) and integral ($K_i$) gains of the controller were set through an iterative process to achieve a fast settling time.

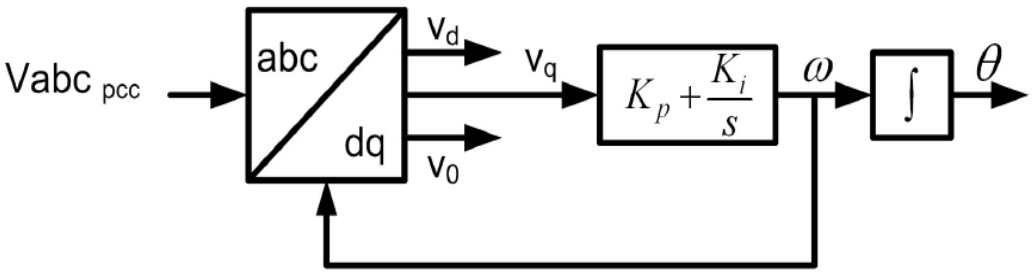


Figure 3.12. Schematic diagram of the phase locked loop (PLL).

The output from the PI controller is the rotation frequency $\omega$ in rad/s. Integrating this term results in the rotation angle θ in radians. The operation of the PLL is governed by

$$\omega = K_P V_q + K_I \int V_q dt$$

$$\theta = \int \omega \, dt$$

### 3.4.4. Dual loop control

A double-loop control strategy is implemented to keep the DC voltage constant and generate pure active power at the same time, and they are realized by outer voltage loop and inner current loop control respectively. To regulate the grid current, there is a fast internal current loop, and an external voltage loop, which controls the dc-link voltage. The current loop is responsible for improved power quality and current protection. The dc-link voltage controller is responsible for balancing the power flow in the system. Usually, the design of this controller aims for system stability having slow dynamics.

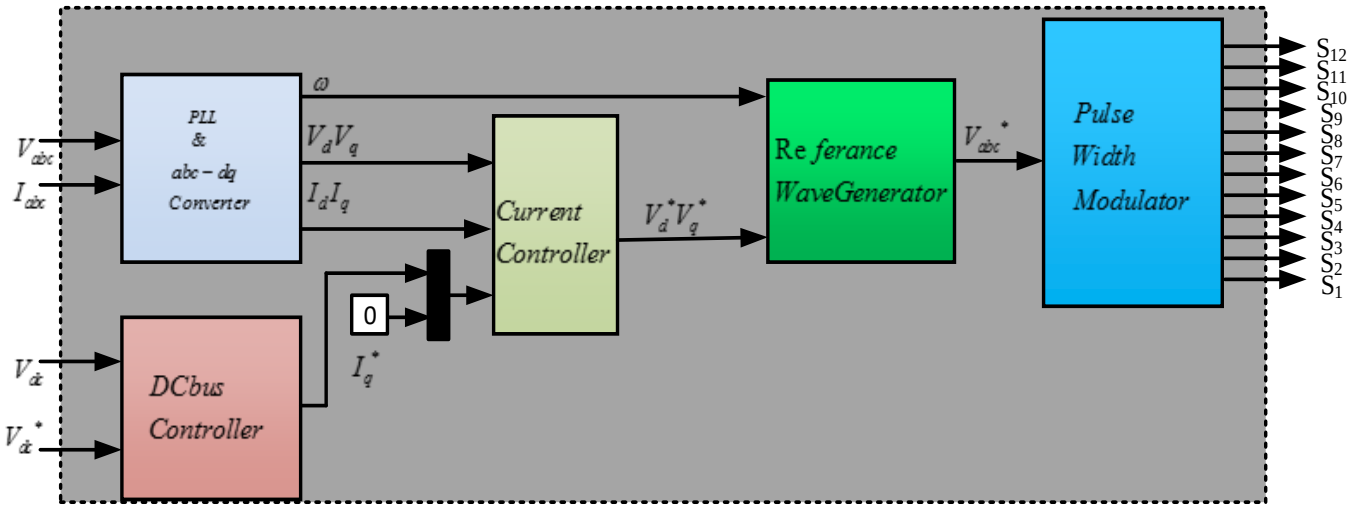


Figure 3.13. Schematic of the control block for grid connected DCMLI

Figure 3.13 represents the schematic of the control strategy for grid connected DCMLI. The control scheme consists of a phase locked loop (PLL), voltage regulator, current regulator, reference wave generator and PWM generator. In the PLL control circuit, the three voltages and currents are converted into *dq0* transformation. Similarly, the voltage regulator (highlighted in figure 3.15) proceed to the current Regulator and $V_d$ and $V_q$ are given to reference wave generator where it can be compared with the phase angle. Further, it is converted into three ($V_{abc}$) only to proceed to PWM Generator to generate the pulses required for the DCMLI.

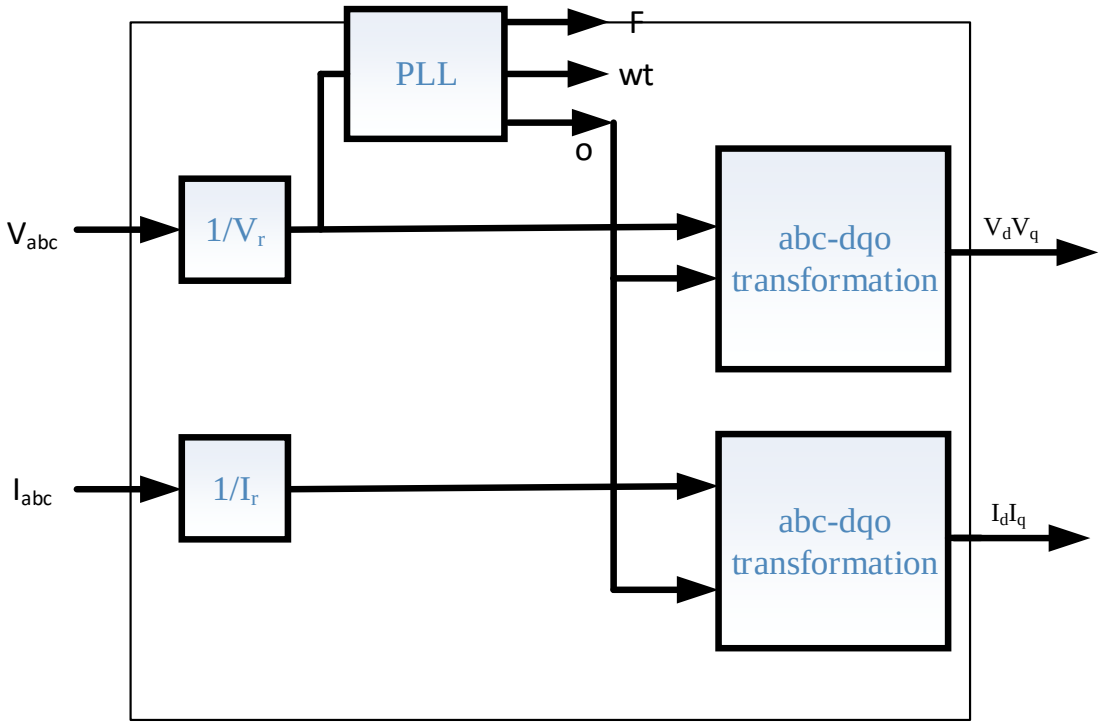


Figure 3.14. Generation of direct and quadrature components.

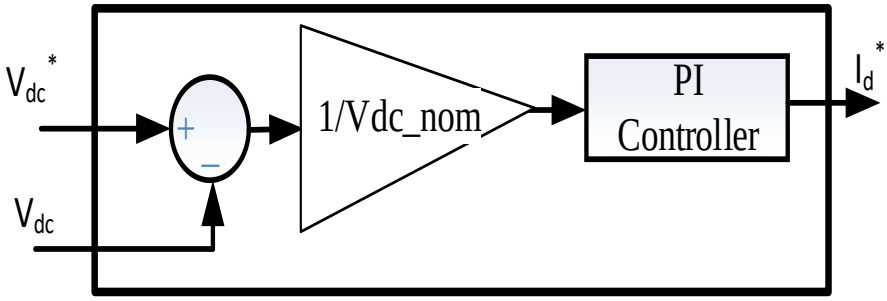


Figure 3.15. DC bus voltage regulator.

***The synchronous reference (dq) frame control***

Synchronous reference frame control, also called *dq* control, uses a reference frame transformation module *abc* → *dq*, to transform the grid current and voltage waveforms into a reference frame that rotates synchronously with the grid voltage. As a result, the control variables are transformed to dc values; thus, filtering and controlling can be easily achieved [14]. A schematic of the *dq* control is represented in figure 3.16. In this structure, the dc-link voltage is controlled in harmony with the necessary output power. Its output is the reference for the active current controller. The reference for the reactive current is set to zero to maintain unity power factor at the inverter output.

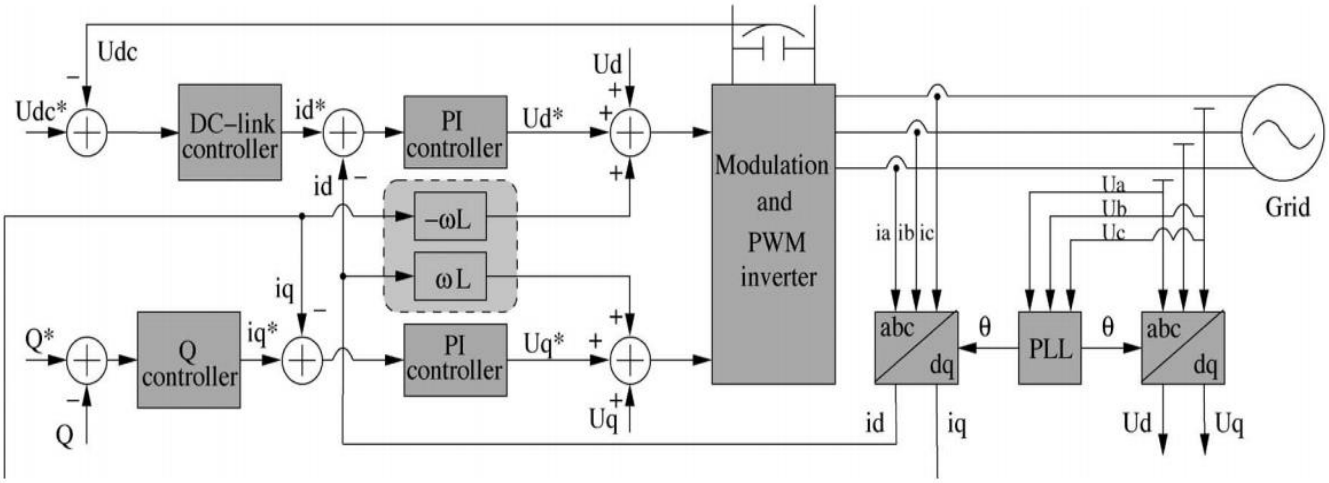


Figure 3.16. General structure for synchronous rotating frame control structure.

# Chapter 4: PROPOSED PV SYSTEM SIMULATION RESULTS

The proposed Photovoltaic Grid Connected System has been successfully designed, modelled and simulated on MATLAB Simulink Environment. In this thesis, a 100KW Solar PV Power generation unit is designed and simulated for both the inverter topologies. Simulink diagrams of three grid connected PV systems are as shown in the figures below.

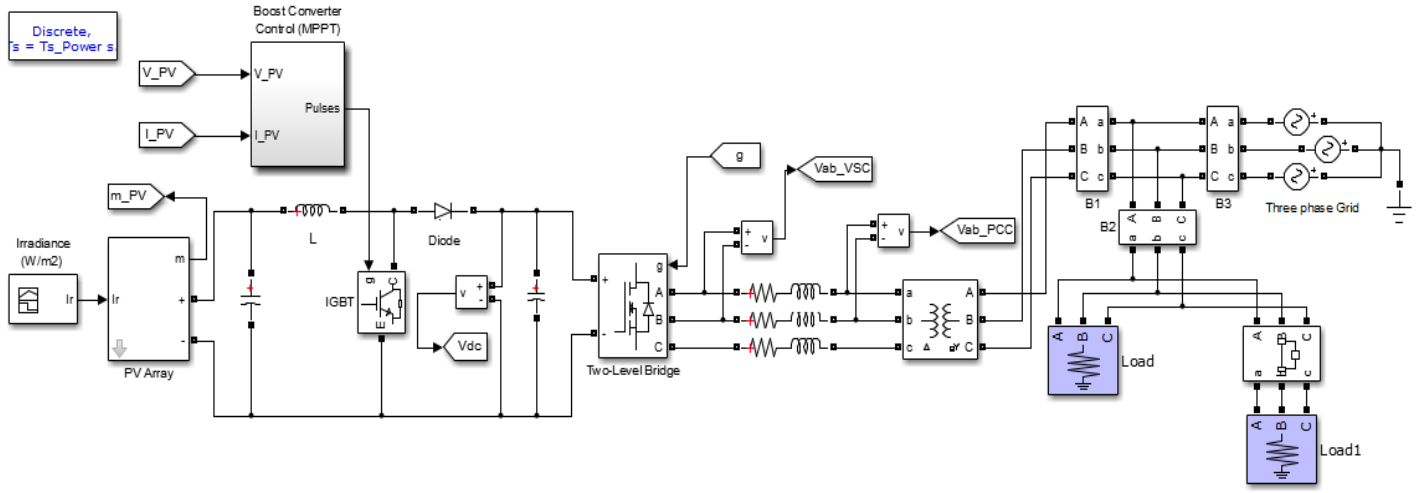


Figure 4.1. Simulink model of grid connected Two-Level Inverter system.

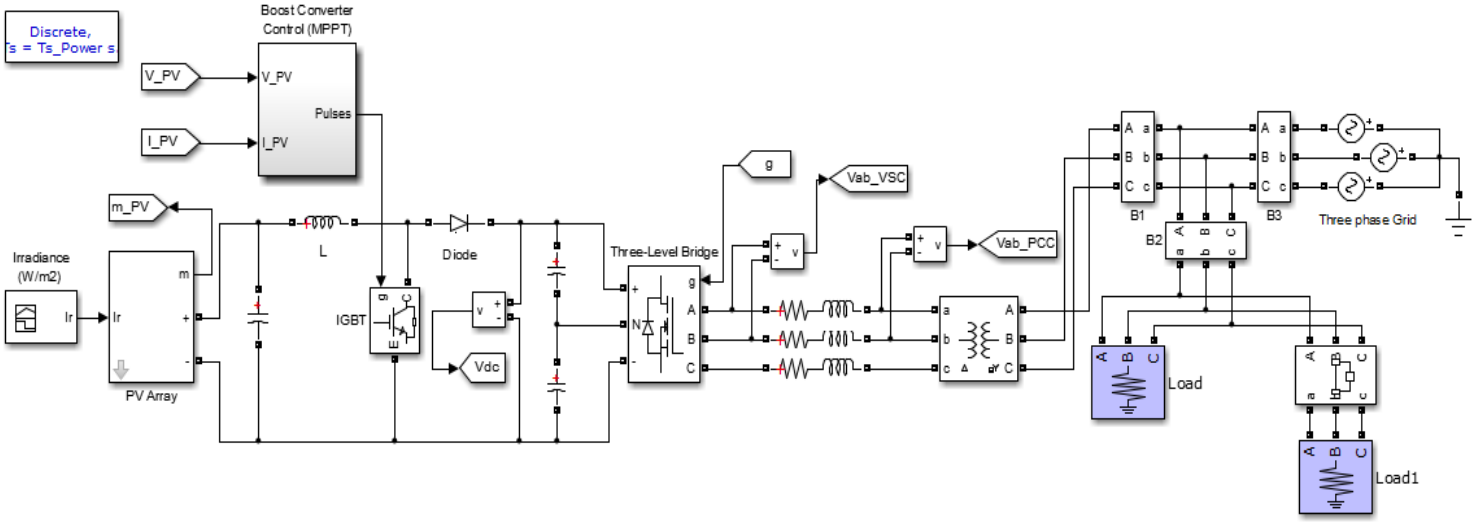


Figure 4.2. Simulink model of grid connected Three-Level Inverter system.

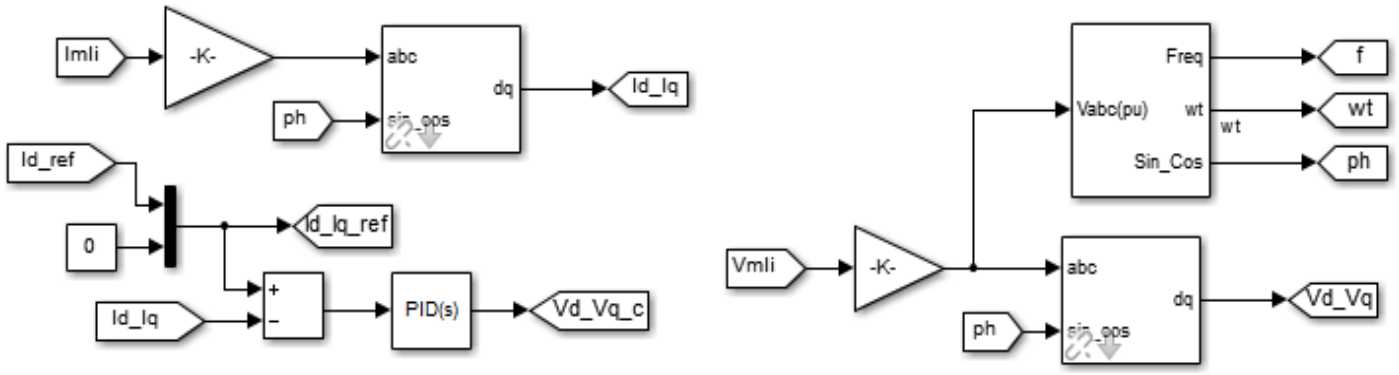


Figure 4.3. Inner current control loop (left) and PLL synchronization (right).

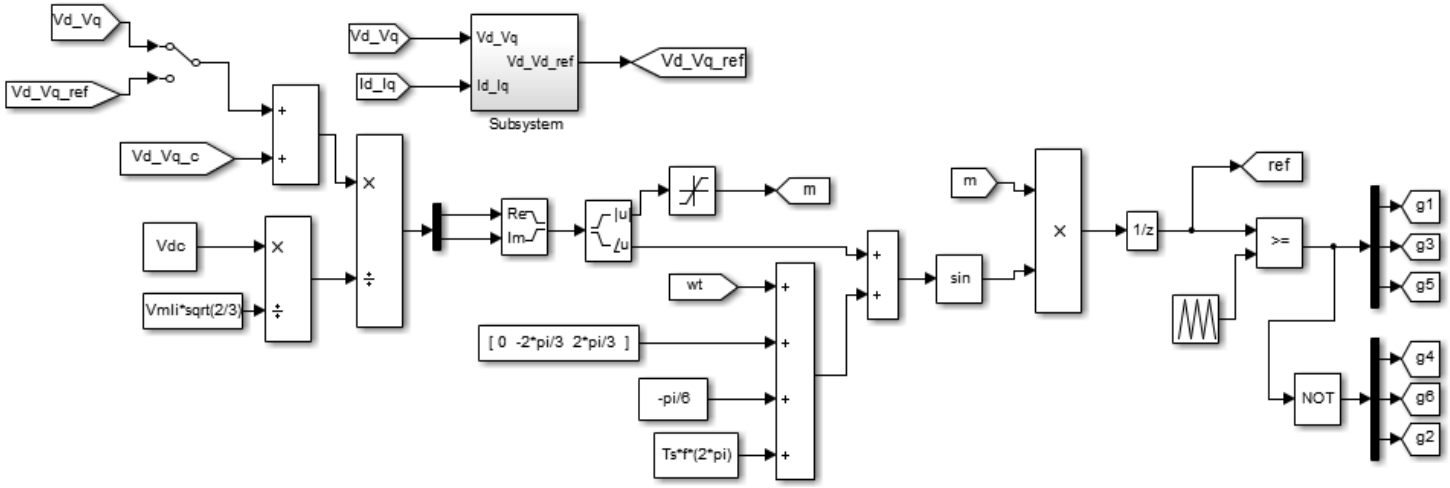


Figure 4.4. Voltage control loop and gate pulses generation for Two-Level Inverter.

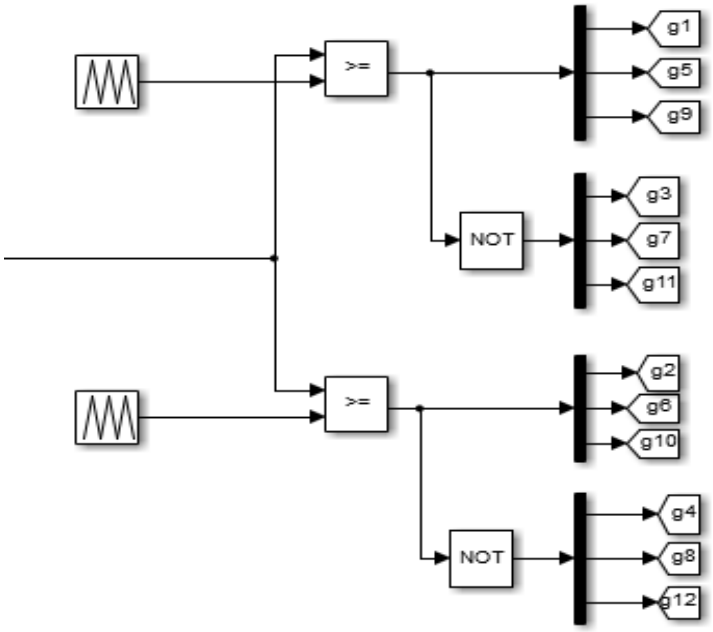


Figure 4.5. Pulses generation for Three-Level Inverter.

The objective is to design 100 kW grid connected PV system to feed the power to 100 kW load under standard test conditions (irradiation, 1000 W/m$^2$), feed the excess power to grid subjected to high irradiation and take the power from grid during lower irradiation condition. Design parameters of such a solar PV array and connection of solar PV module are mentioned as table 4.1.

Module Type: Maharshi Solar-130.

| Data Sheet Values | | Estimated Parameters | |
|---|---|---|---|
| $I_{sc}$ (Short circuit current) | 5.82 A | $I_{ph}$ (Photon current) | 5.9602 A |
| $V_{oc}$ (Open circuit voltage) | 44.11 V | $I_0$ (diode current) | 0.0312 µA |
| $V_{mpp}$ (Voltage at maximum power) | 35.62 V | $A$ ( Diode factor) | 1.30 |
| $I_{mpp}$ (Current at maximum power) | 3.595 A | $R_s$ (series resistance) | 0.038 Ω |
| $N_s$ (No. of Series connected solar cells) | 96 | $R_{sh}$ (Shunt resistance) | 993.5 Ω |
| Temperature Coefficients | | | |
| $K_i$ (Temperature Coefficient for current) | 0.015% | $K_V$ (Temperature Coefficient for voltage) | -0.21% |

Table 4.1. Design specifications of Solar PV Module.

***Design Specifications of PV String***

No. of Series Modules $N_{sm}$ = 7 for 250V DC range at 1000W/m$^2$ and 25°C

No. of strings in Parallel $N_{pm} = \frac{100000}{(249.34*7)} = 58$.

DC-DC Boost converter is designed along with MPPT Algorithm to track Maximum Power Point from the module. DC-DC Boost converter is selected so as to increase the voltage output voltage of the module which is around 250V at standard test conditions. Temperature and irradiation is of varying nature and results variable nature DC power at output terminals of PV array. DC-DC Converter is designed and placed after PV array to serve two purposes, namely, voltage boosting (Increases the voltage level of ripple free or low ripple content) and MPP tracking.

For these objectives DC-DC boost converter is designed as follows using following specifications of the system.

Input Power of Converter=100 kW (equal to array output power)

Input Voltage range of Boost Converter = 200V to 250V (under varying atmospheric conditions)

Nominal output voltage = 850 V (required DC bus voltage level to produce output voltage, which is equal to transformer input voltage)

Maximum output current = $\frac{100\,kW}{850\,V} = 117.65\,A$

Switching Frequency of the DC-DC Converter = 10 kHz

Decoupling Capacitor:

Ripple factor= $r = 0.02\% = \frac{1}{4\sqrt{3} f_s C R_{in}} \Rightarrow C \approx 1000\,\mu F$

***Calculation of the Boost Converter Parameters***

Calculation of the Inductor Value: To find out this maximum switch current duty cycle (D) is a key parameter, it is calculated for the minimum input Voltage. Since minimum input voltage leads to maximum switch current.

$$D = 1 - \frac{V_{in(\min)} * \eta_{boost}}{V_{out}}$$

For $\eta_{boost} = 100\%$ duty cycle $D = 1 - \frac{V_{in(\min)}}{V_{out}} = 0.76$

$$\Delta I_L = 1 - \frac{(V_{in(\min)} * \mathrm{D})}{F_s * L} \Rightarrow \frac{(V_{in(\min)} * \mathrm{D})}{F_s * \Delta I_L} = \frac{R_L (1 - D)}{2 * F_s}$$

To find out the inductor value inductor ripple current need to be estimated. For the 20% of the load current, the inductor ripple current= $\Delta I_L = 0.2 * I_{out(\max)} * \frac{V_{out}}{V_{in}}$

Inductor Value= $3.1250e^{-05} H$

Calculation of Maximum Switch Current: It is clear that, in case of the boost dc-dc converter main switch is maximum current can be calculated as follows,

$$I_{SW\,MAX} = \frac{\Delta I_L}{2} + \frac{I_{out\max}}{1 - D}$$

Blocking voltage of the switch, $V_o$ = 850 V

Rectifier Diode Selection: Diode current=Diode Voltage

Calculation of the Capacitor Value: $$c = \frac{I_0 * D}{\Delta V_0 * F_s} F$$

As this project one of the objective is to provide 100 kW to the grid from a PV system. In order to control the power using the MPPT control, a synchronous field oriented control based PI controller is designed to control the inverter and the outcome from the inverter results have been presented below.

The system is simulated for 2 seconds. Initially, irradiance is set at 1000 W/m$^2$. The conditions at different points of time during the simulation and events occurring during the simulation is shown in table 4.2.

| S.No. | Time(s) | Condition | Event |
|---|---|---|---|
| 1. | 0 – 1 | 100% solar power, 200 kW load | 100 kW supplied by PV, 100 kW supplied by grid |
| 2. | 1 – 1.5 | 75% solar power, 200 kW load | 75 kW supplied by PV, 125 kW supplied by grid |
| 3. | 1.5 – 2 | 75% solar power, 100 kW load | 75 kW supplied by PV, 25 kW supplied by grid |

Table 4.2. Simulation events timeline.

These results have been presented here for 100% loading during 0-0.5Sec, 50% loading during 0.5Sec-1Sec and also applied line change of 25% during load change means 75% of input power during 0.75Sec-1Sec. It is clearly understood that during 0.75Sec-1Sec there is both load as well as line change both applied simultaneously.

All these cases, the results are observed at various points such as inverter output terminals, PCC, load terminals and grid terminals for better analysis of proposed system. At each node, voltages, currents and power are shown distinctly with the help of following figures. Moreover, for the better justification of power quality, THD analysis is carried out and presented at each node. Specifically, PCC voltage and currents will decide the power quality of converter. The zoomed in view some results are carried out for better understanding about results.

## 4.1. Results for Three Phase Two Level Inverter

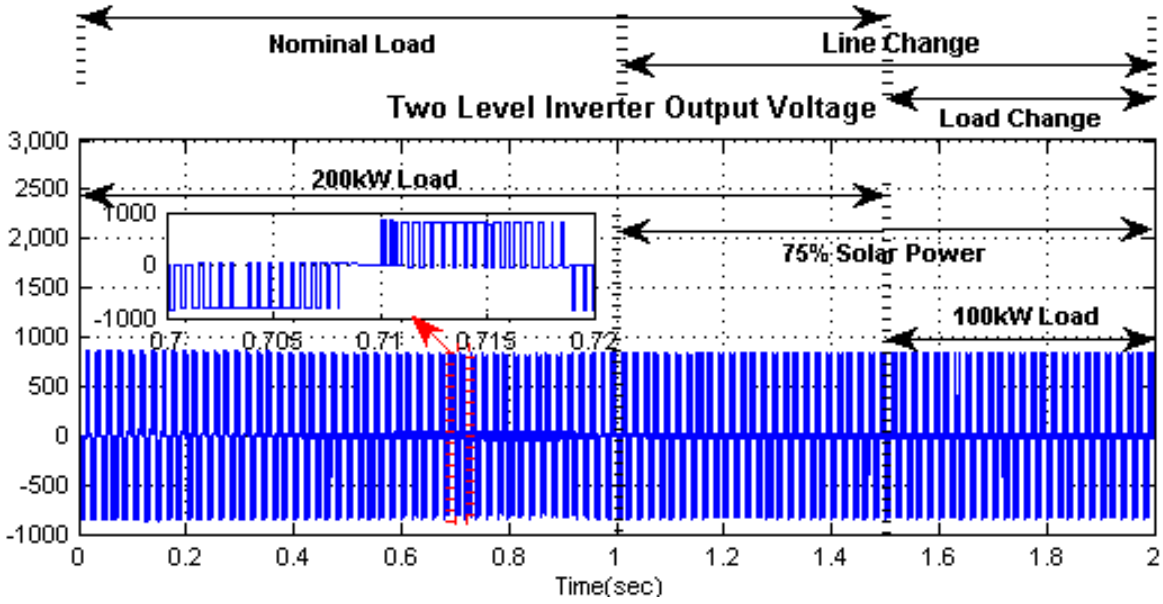


Figure 4.6. Two-Level Three Phase Bridge inverter (TPBI) output voltage.

Figure above shows the inverter output voltage of two-level inverter. The load sharing of PV module and grid with relation to voltage is also mentioned. When the load is 200 kW, the inverter bears the load which is shown with respect to time in seconds. The TPBI (Three Phase Bridge Inverter) output voltage is presented and it can be observed that line to line voltage of TPBI has three voltage levels and it can be inferred that there is no distortion even for load and/or line variations. In all the conditions namely, normal, load, line and reference signal variations, the inverter is able to produce constant output voltage throughout the operation as one of the requirements is maintaining constant voltage for grid interfacing. This is achieved through the proper operation and control of inverter.

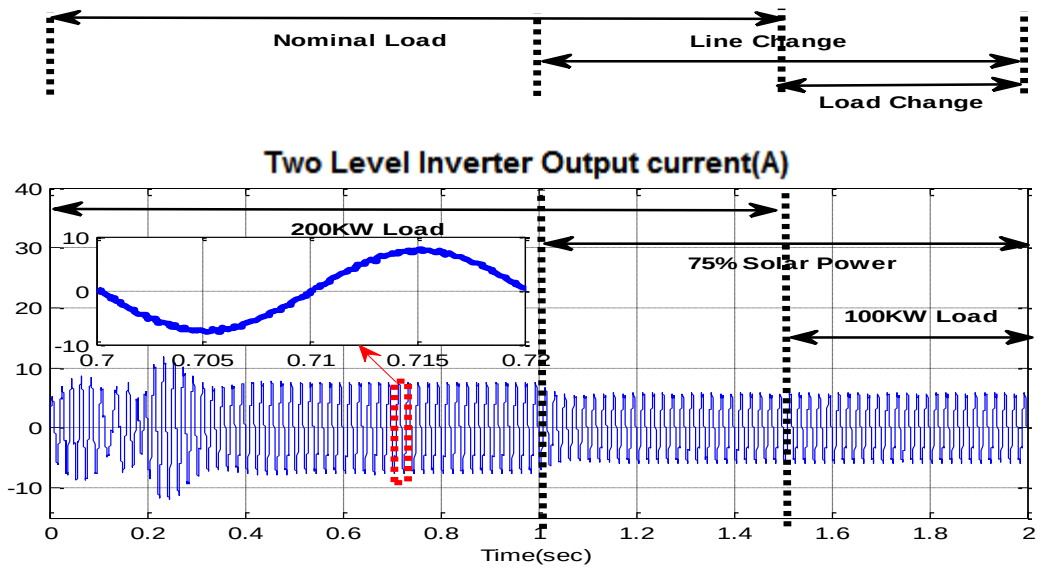


Figure 4.7. Three phase bridge inverter (TPBI) output current.

Inverter output current is shown in the above figure. The same current is flowing through the coupling reactor and available PCC to feed the grid and/or load depending on the operating conditions. From this figure, it can be inferred that inverter current is nearly sinusoidal due to low harmonic content as shown, which is suitable for grid/load requirements. For crucial analysis about harmonic content, THD analysis is carried out and presented later.

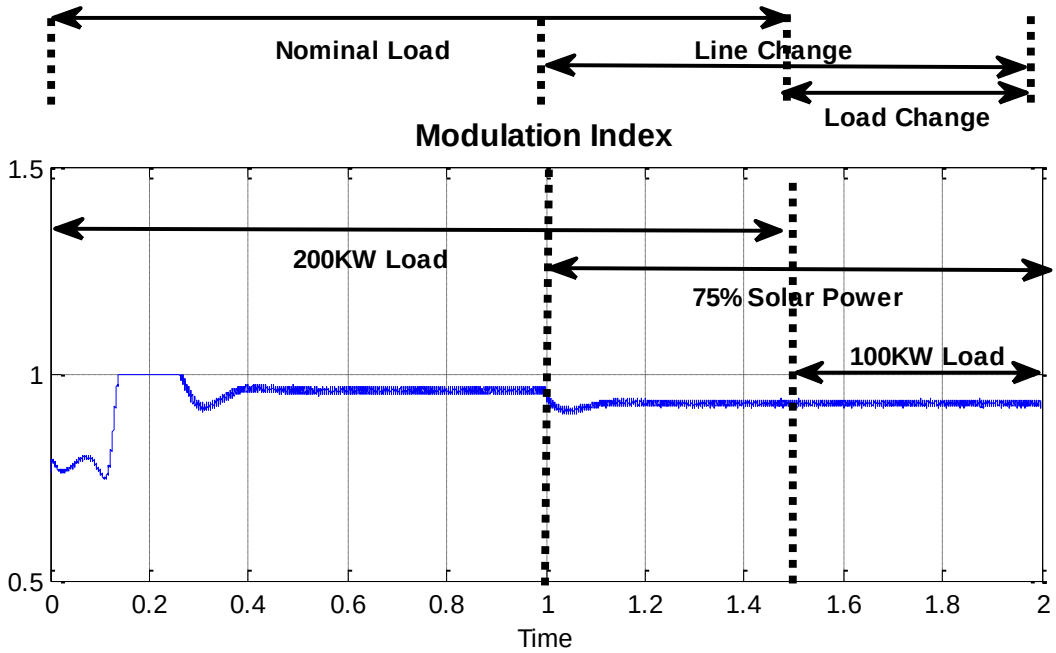


Figure 4.8. Modulation index of TPBI inverter.

Modulation index of this closed loop inverter control is presented above. The figure above demonstrates rapid adjustment of modulation index to meet the system requirements.

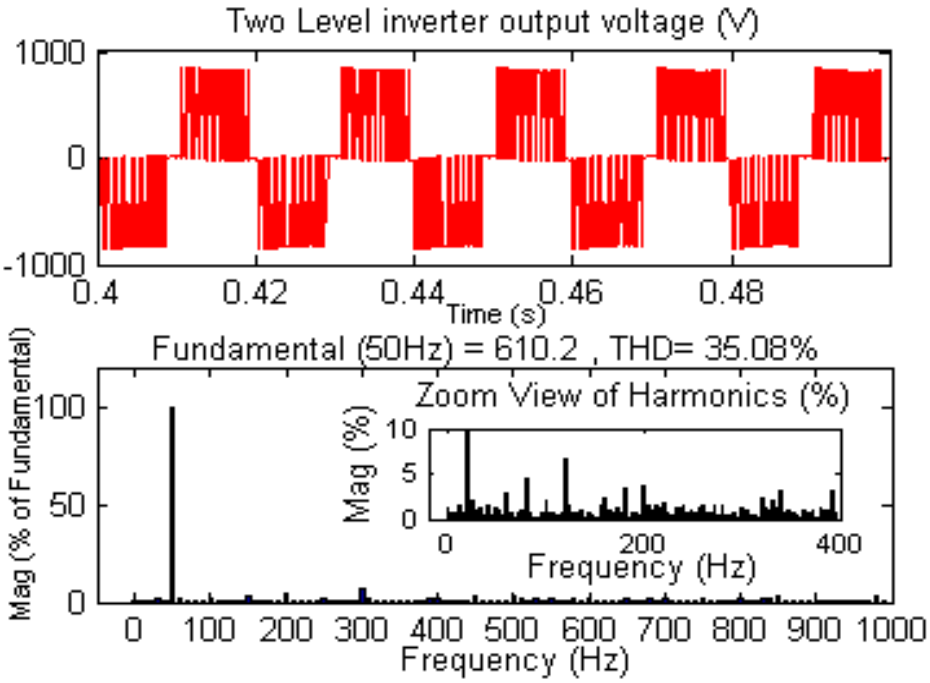


Figure 4.9. Harmonic analysis of TPBI inverter output voltage.

In order to evaluate the power quality of the inverter, THD analysis of inverter output voltage is carried out and its waveform is presented above. From the figure we can deduce that low harmonic content is present at the output of inverter terminals, hence, a low value of coupling inductor is sufficient to suppress the harmonics as per IEEE 1547 standards.

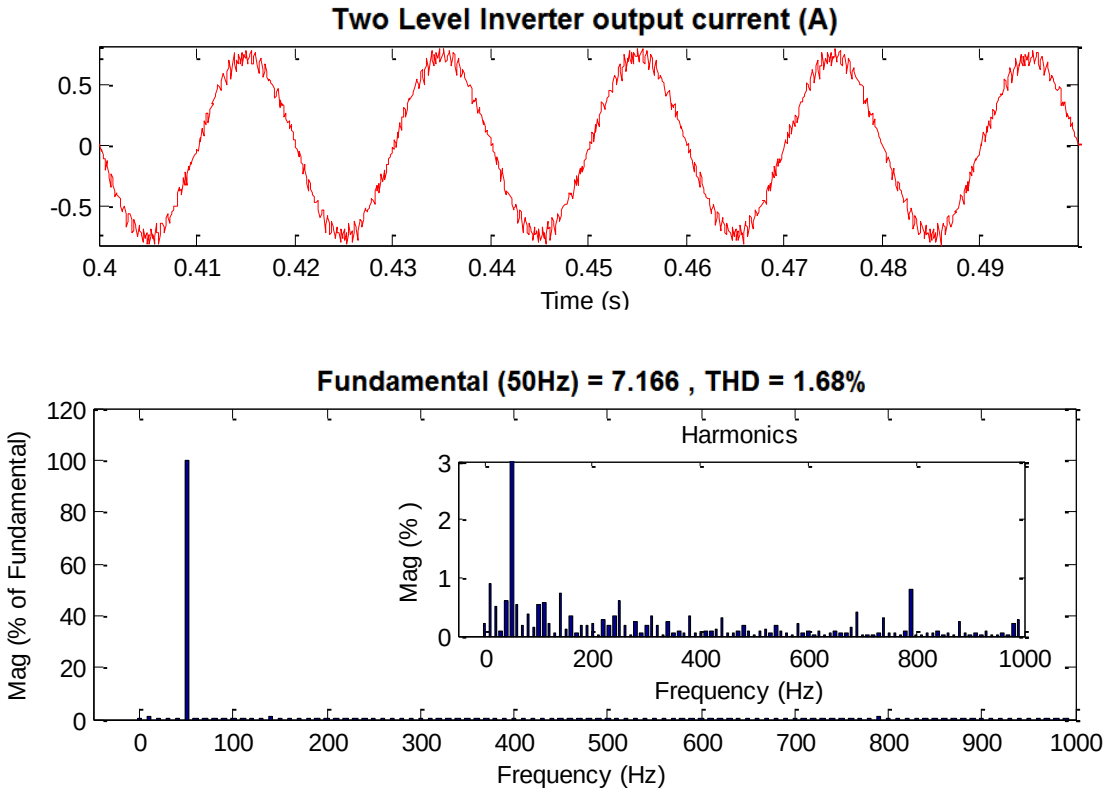


Figure 4.10. Harmonic analysis of TPBI inverter current.

THD analysis of inverter output current is carried out as shown in the above figure. The output current of inverter is injected into grid through the coupling reactor. From this waveform, it is evident that output current which is flowing through the PCC to grid having THD of 1.68% is clear indication of at par inverter design, offering good quality of power to grid. From zoom in view of the figure, it is clear that except fundamental component of current no other order frequency component is having even 2% contribution. This demonstrates sophisticated performance of the designed controller. Further, the designed power converter's controller offers a robust performance for power quality issues since offers a low THD of current under load, line and reference varying conditions also.

All the above results are only possible due to proper tracking of reference value. The results presented below demonstrates the tracking of reference value. As one sees the below figure, the results presented here have following changes in the value of d-axis current component:.

- From 0s to 1s, $I_d = 1$, as insolation is 1000 W/m$^2$ during this time interval. Load is double the power output from PV. So, half the load is supplied by grid.

- From 1s to 2s, $I_d$ = 0.75, as insolation is 750 W/$m^2$.

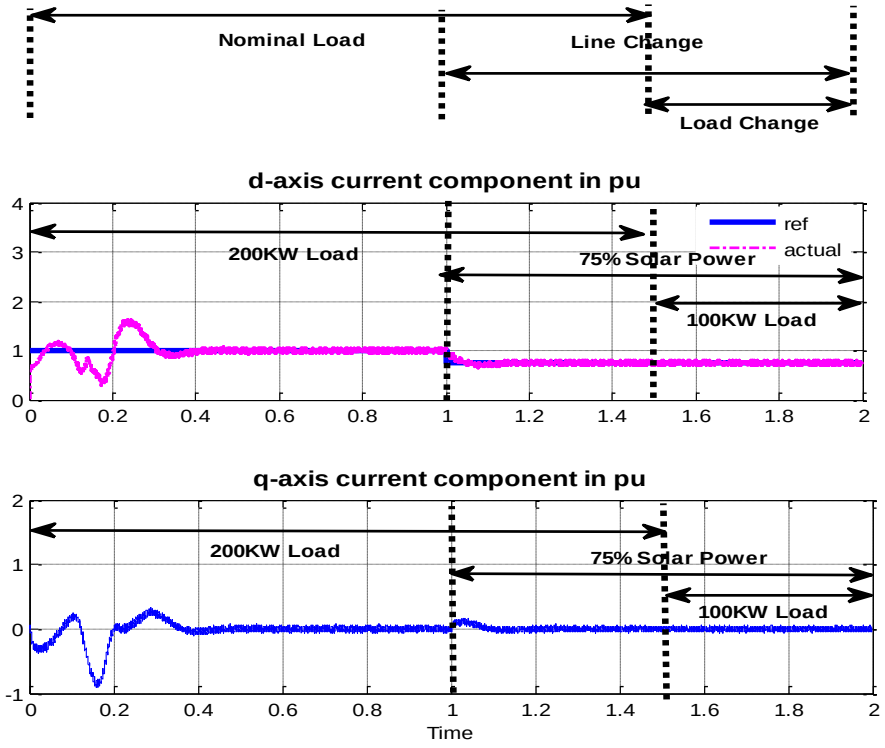


Figure 4.11. Current components of d-axis and q-axis under load and line changes.

The figure above shows both the d-axis and q-axis currents (pu) explaining the effect of changing load and line on injected currents. From the q-axis waveform it can be observed that reactive component of current is always zero, which is desired during any disturbances injected at input and load. Disturbance rejection of by the controller is highly appreciated and unity power factor operation is achieved at PCC. The d-axis current component, which is responsible for active power, is tracking the reference without any steady state error. Hence, inverter modulation index and reference waves are generated more accurately, which in turn generates gate signals to inverter switches resulting in accurate output at the load terminals.

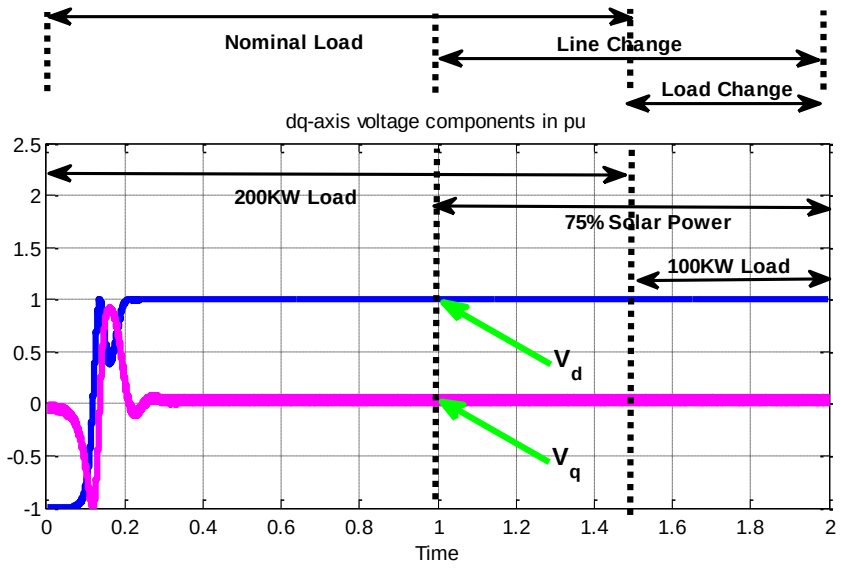


Figure 4.12. dq-axis voltage components under load and line changes.

dq-axis voltage components are shown in figure above. These are used to generate reference modulating signals to synthesize the modulating signal along with modulation index.

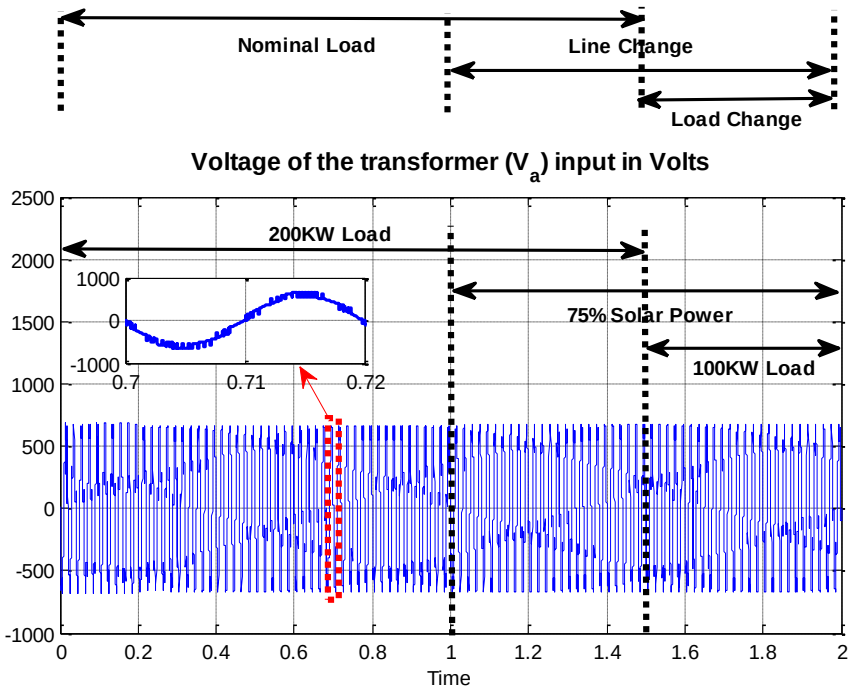


Figure 4.13. Voltage of the transformer input in volts under load and line changes.

The voltage at the output of coupled inductors is same as the step up transformer (400V/11000V) input terminals voltage, as shown in the figure above. It can be noted that voltage at transformer input terminals has low harmonics. Hence, the power conditioning system offers high quality of voltages and currents to the utility.

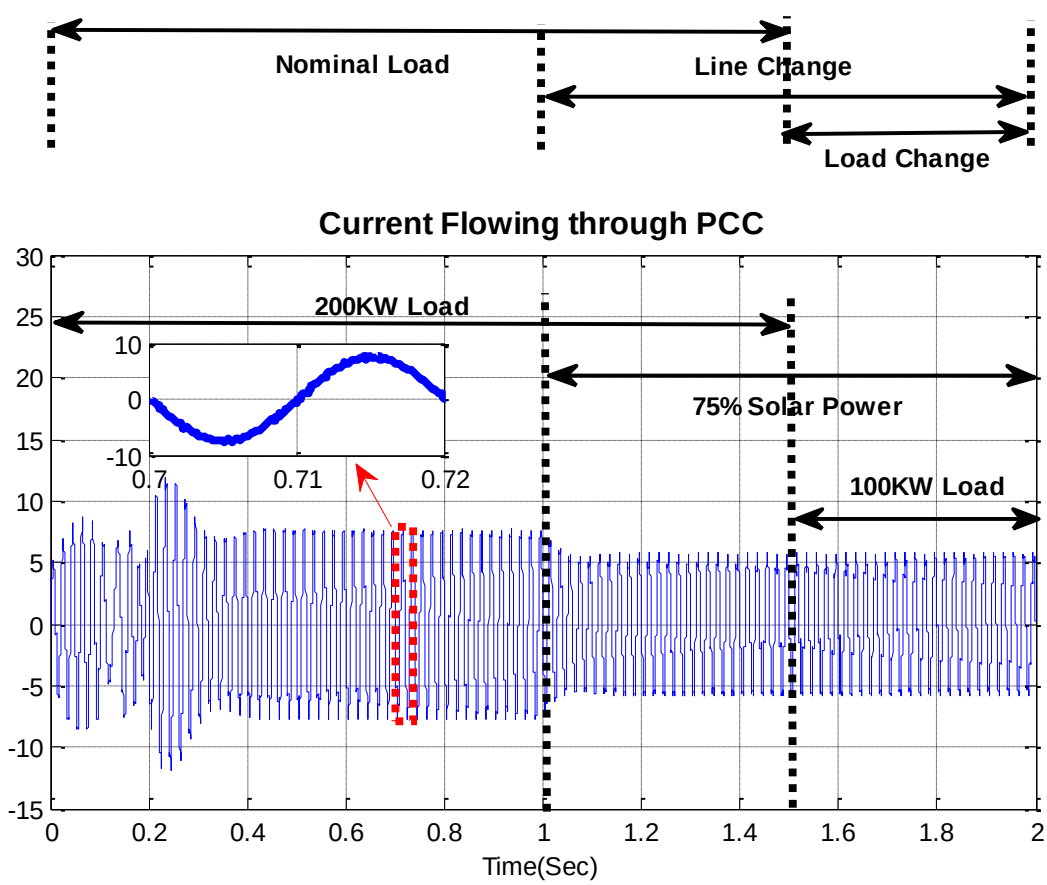


Figure 4.14. Current flowing through PCC under load and line changes.

Figure above highlights the current flowing through the PCC as shown demonstrates the change of current flow (nominal load is 100kW). When 75% of the load is served by PV, the rest of the load is shared by the grid. When more load is shared by the PV, the load on the grid decreases and vice versa.

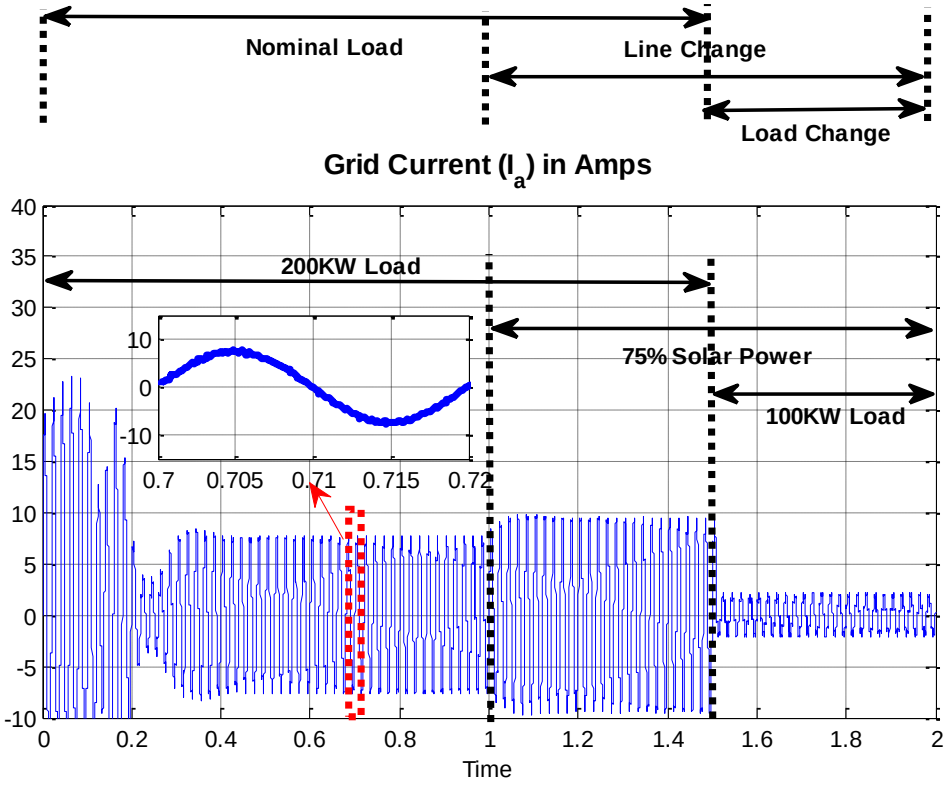


Figure 4.15. Grid current under load and line changes.

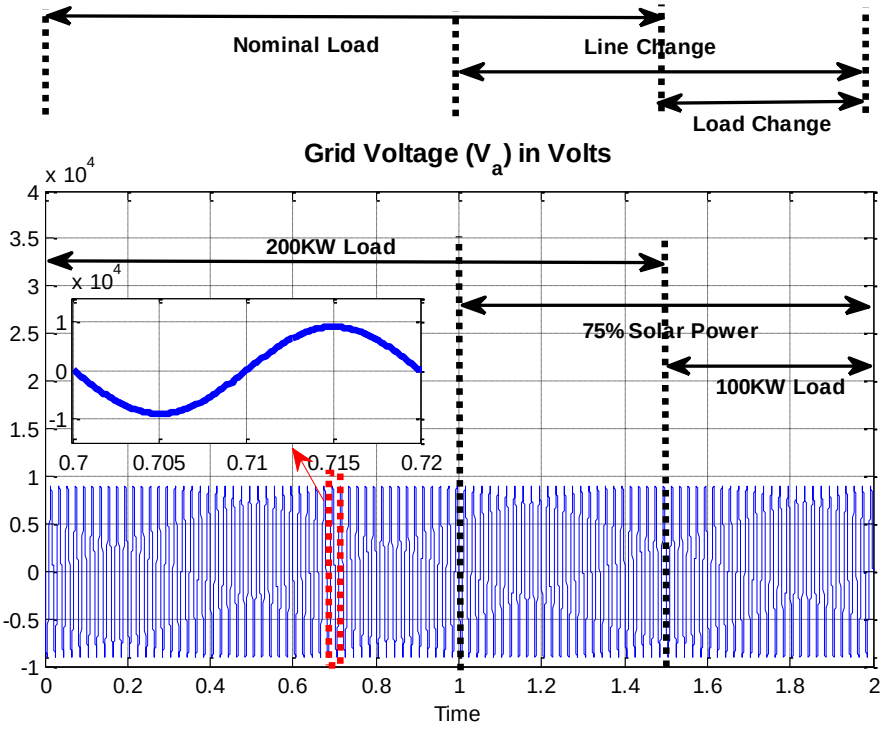


Figure 4.16. Grid voltage under load and line changes.

The flow of current is explained in Fig. 4.16, while the grid voltage variation is shown in Fig. 4.17. A clear picture of the solar inverter/converter system emerges when comparison is made between the flow of voltage and current in the grid.

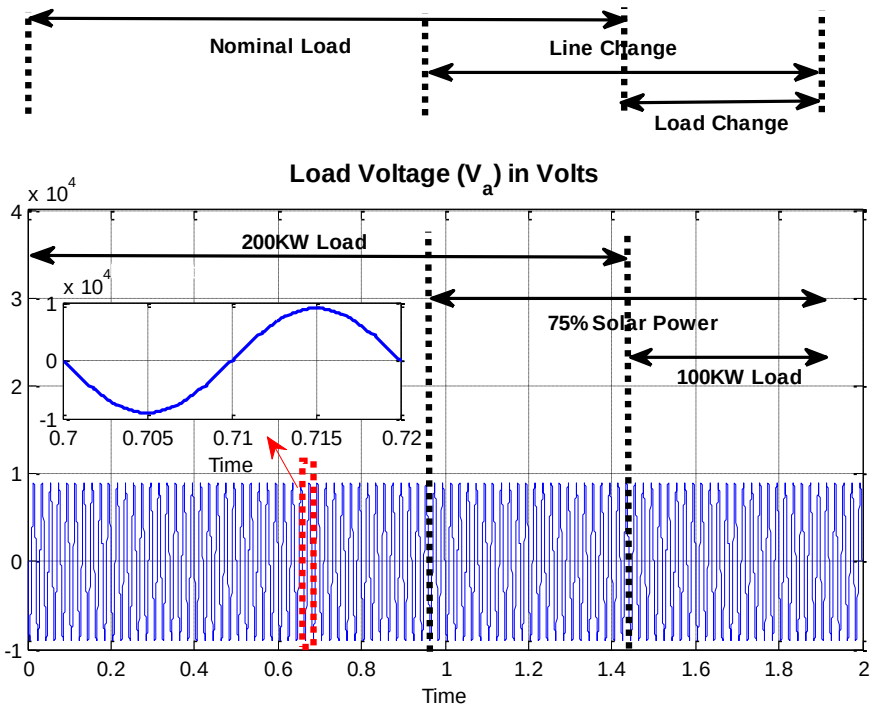


Figure 4.17. Load voltage under load and line changes.

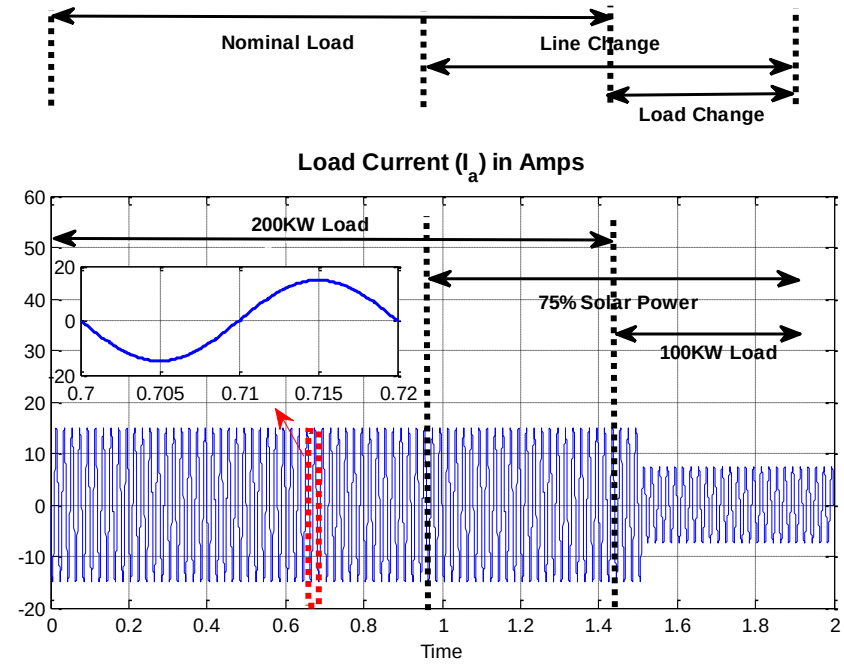


Figure 4.18. Load current under load and line changes.

Figure 4.17 represents the load voltage sharing in correspondence with line and load change against the nominal load which is a fixed point. Load current in Amps is presented in Figure 4.18.

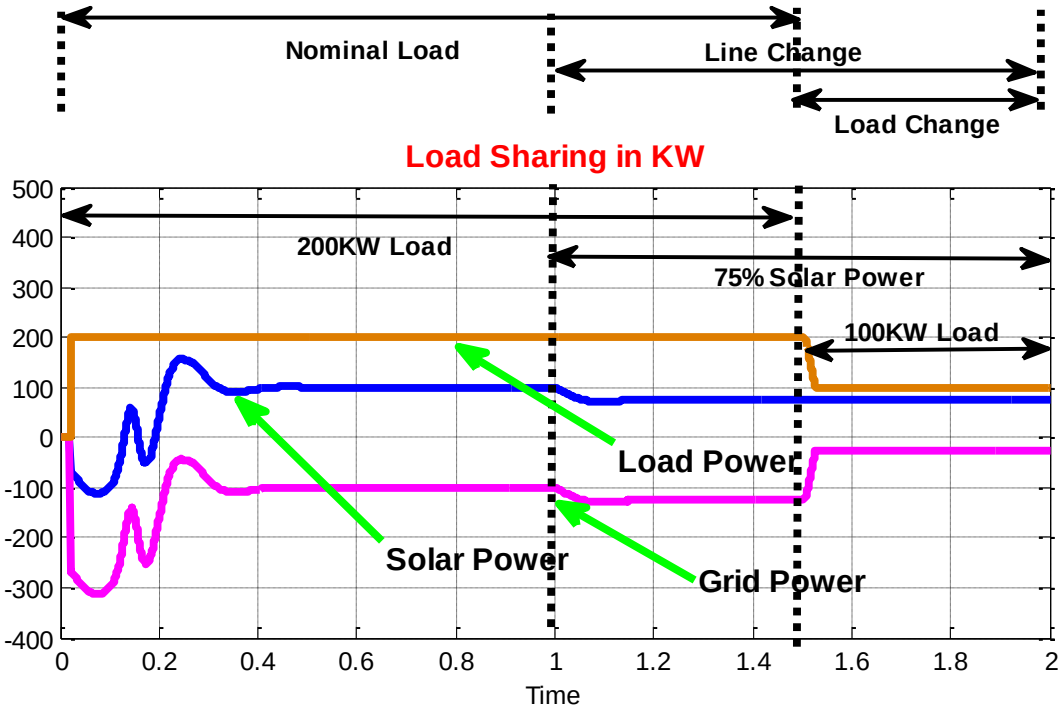


Figure 4.19. Load sharing in kW under load and line changes.

In Fig. 4.19, load sharing among PV and grid is demonstrated. When the load increases, dependence on grid power increases; when the load is less, dependence on solar power decreases. The gap and impact of line change and load change is also shown.

## 4.2. Results for Three Phase Three Level DCMLI

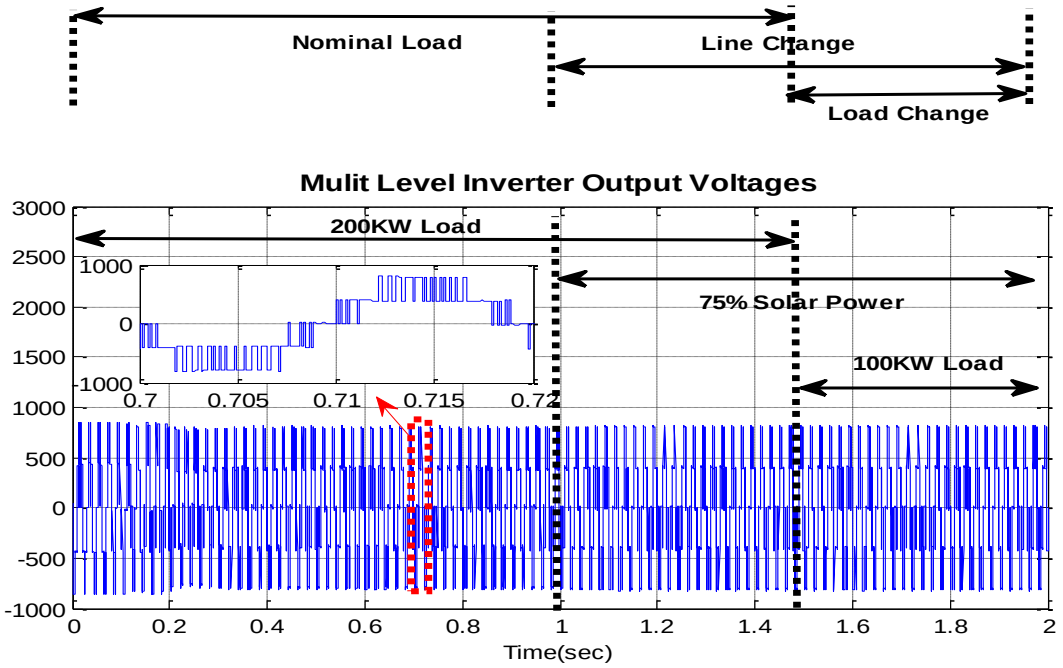


Figure 4.20. Three-Level DCMLI output voltages.

Figure above shows the inverter output voltage of three-level inverter. It can be observed that line to line voltage has five voltage levels and it can be inferred that there is no distortion even for load and/or line variations. Similar to the previous cases, the inverter is able to produce constant output voltage throughout its operation.

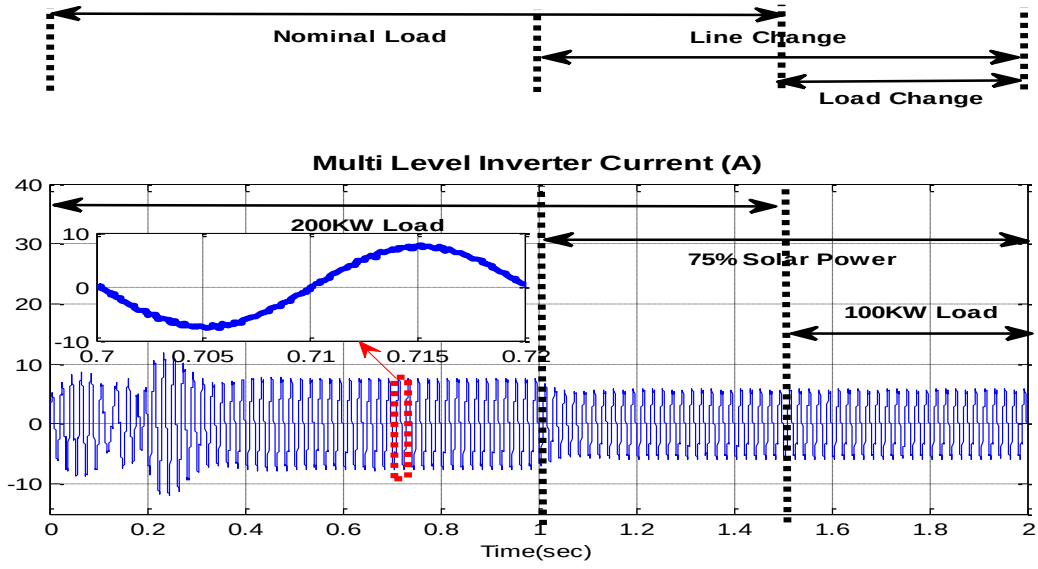


Figure 4.21. Three-level DCMLI output current.

Inverter output current is shown in the above figure. Inverter current is nearly sinusoidal due to low harmonic content as shown.

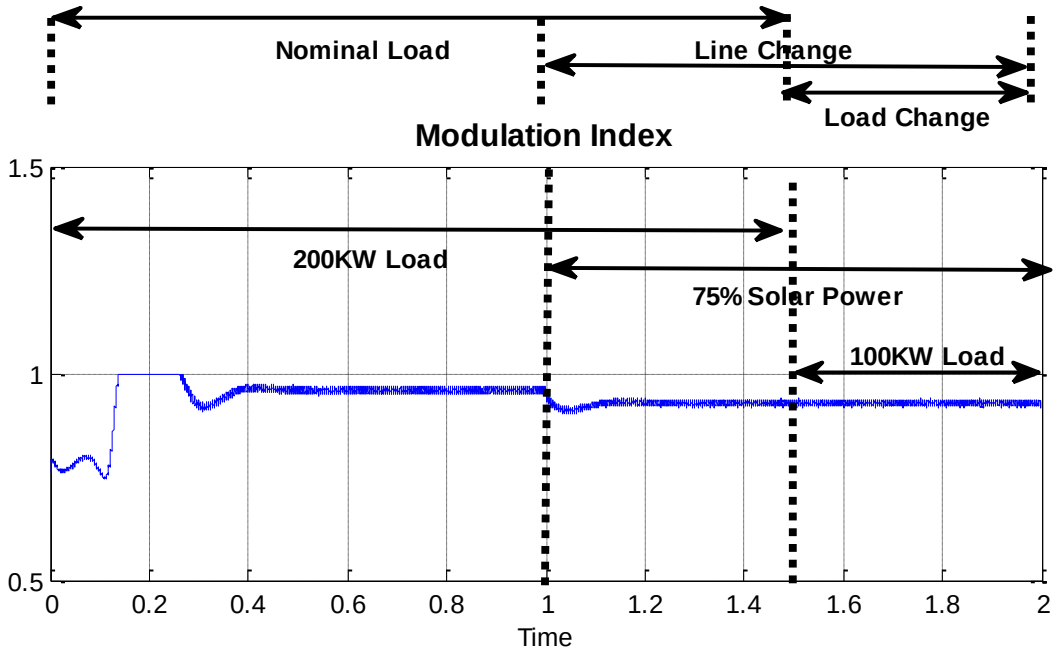


Figure 4.22. Modulation index of three-level DCMLI.

Modulation index of this closed loop inverter control is presented above. The figure above demonstrates rapid adjustment of modulation index to meet the system requirements.

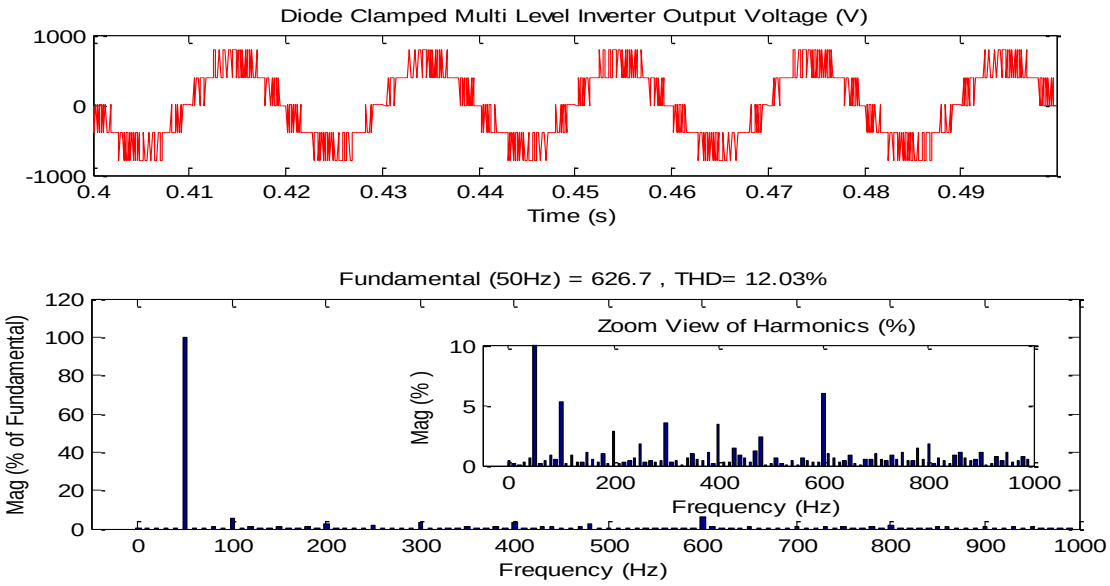


Figure 4.23. Harmonic analysis of three-level DCMLI output voltage.

THD analysis of inverter output voltage is carried out and its waveform is presented above. From the figure we can deduce that low harmonic content is present at the output of inverter terminals, lower than the two level inverter THD (35.08%), which is clear indication of better voltage waveform quality.

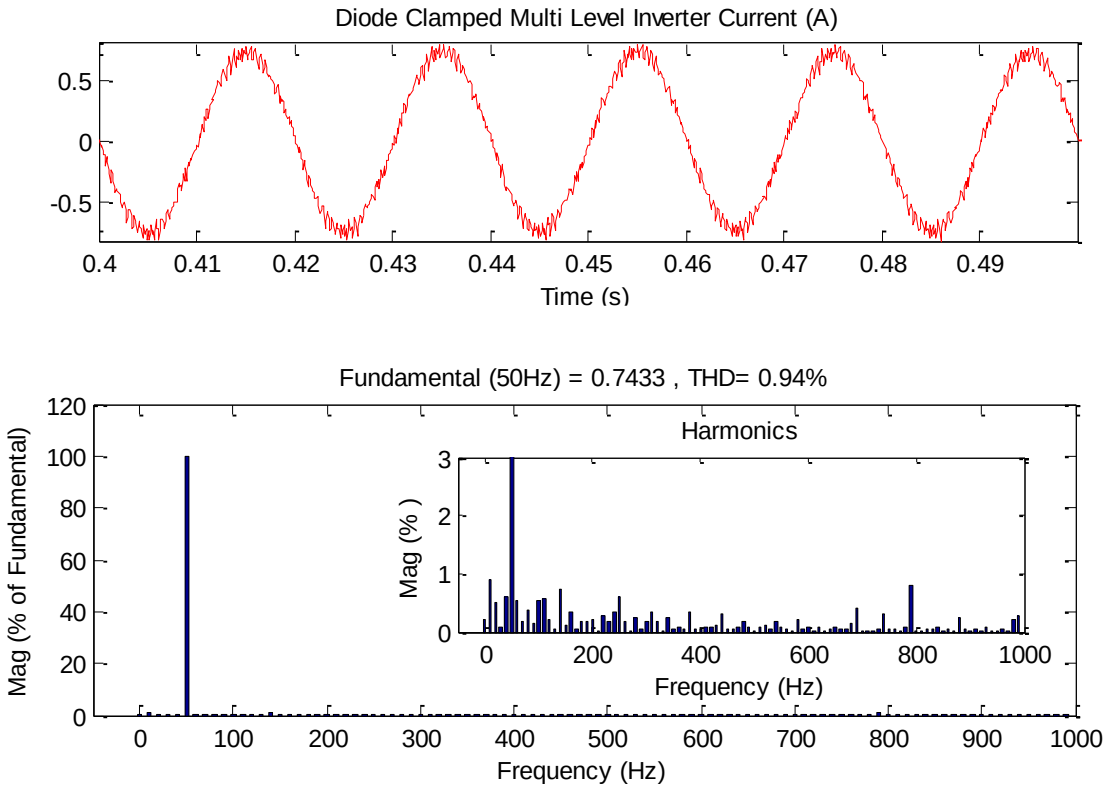


Figure 4.24. Harmonic analysis of three-level DCMLI output current.

THD analysis of inverter output current is carried out as shown in the above figure. From this waveform, it is evident that output current which is flowing through the PCC to grid having THD of 0.94% which is lesser than the two-level topology (1.68%). From zoom in view of the figure, no other order frequency component is having even 1% contribution.

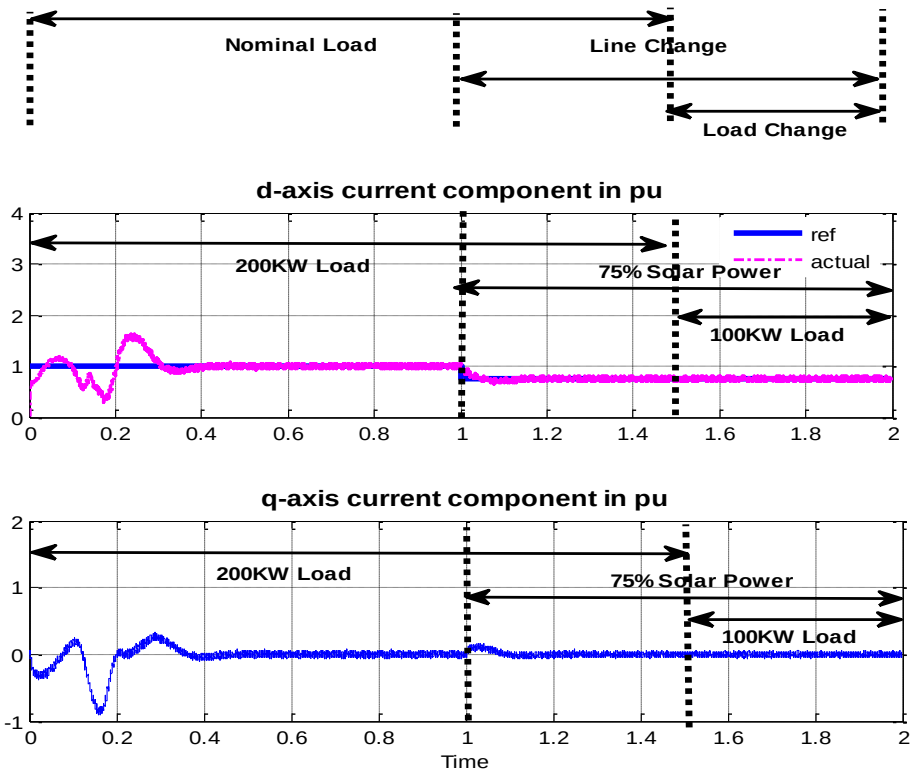


Figure 4.25. Current components of d-axis and q-axis under load and line changes.

The figure above shows both the d-axis and q-axis currents (pu) explaining the effect of changing load and line on injected currents, while figure below shows d-axis and q-axis voltages. These waveforms are as expected as explained in previous sections.

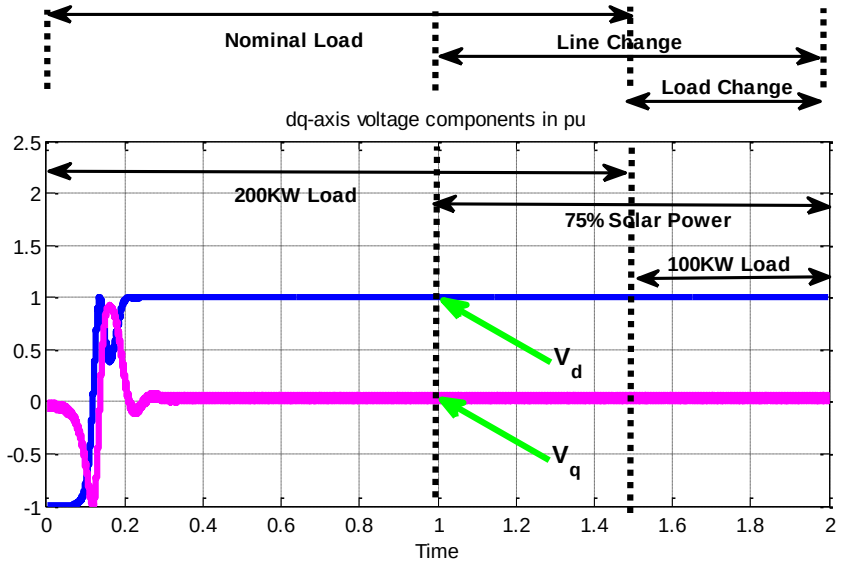


Figure 4.26. dq-axis voltage components under load and line changes.

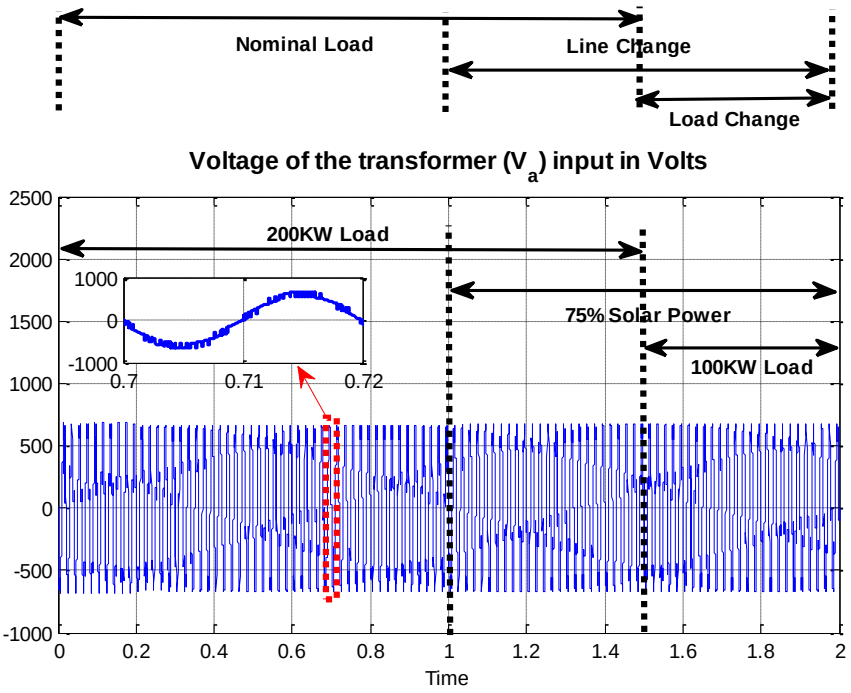


Figure 4.27. Voltage of the transformer input in volts under load and line changes.

The voltage at the output of coupled inductors or the step up transformer (400V/11000V) input terminals voltage, as shown in the figure above.

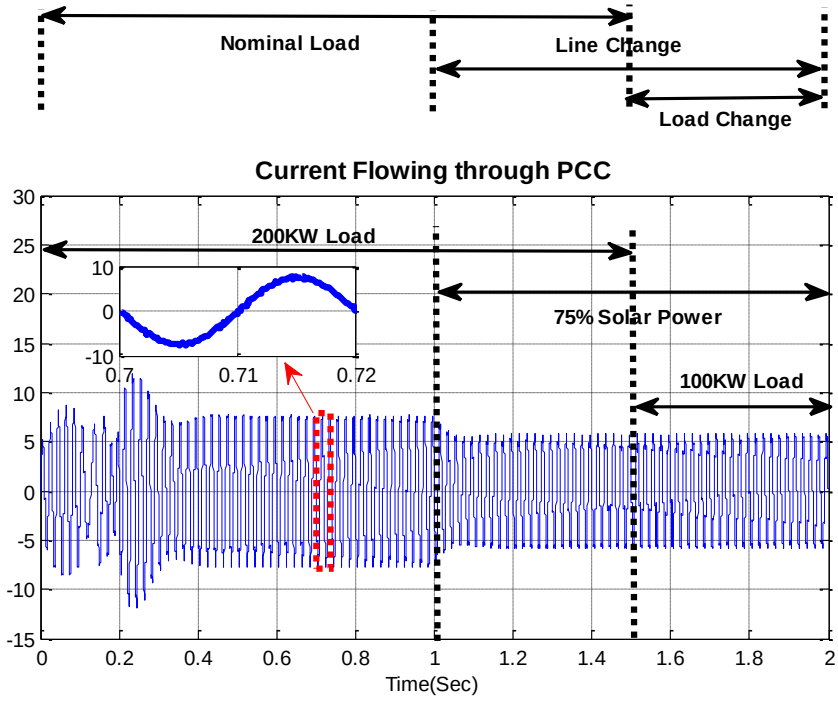


Figure 4.28. Current flowing through PCC under load and line changes.

Figure above highlights the current flowing through the PCC as shown, demonstrating the change of current flow.

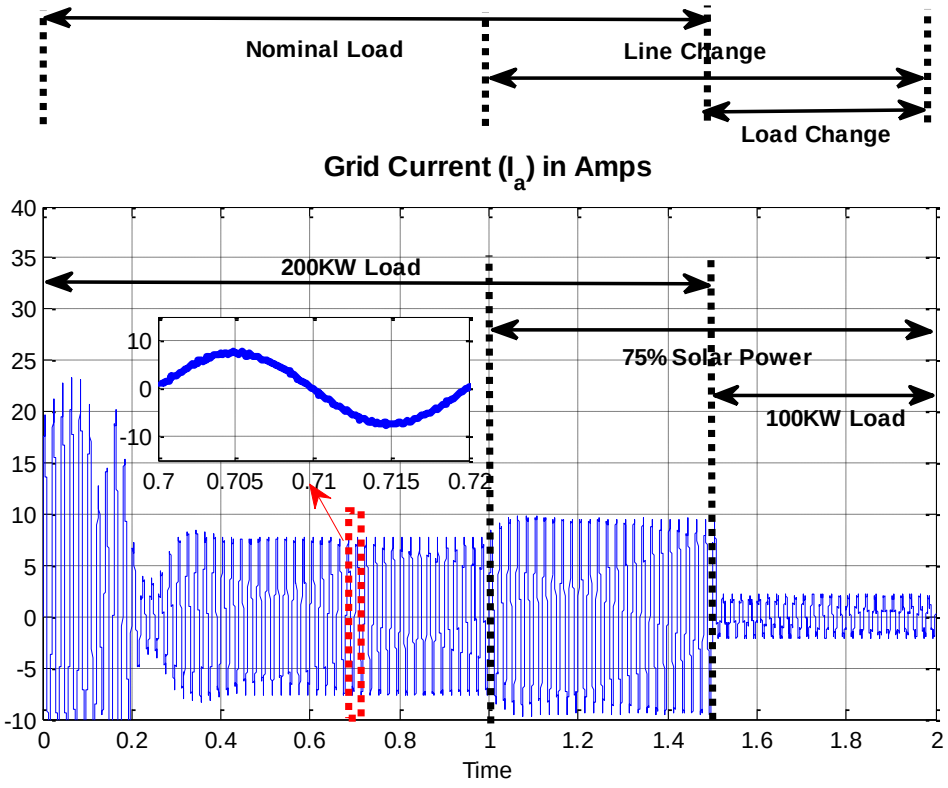


Figure 4.29. Grid current under load and line changes.

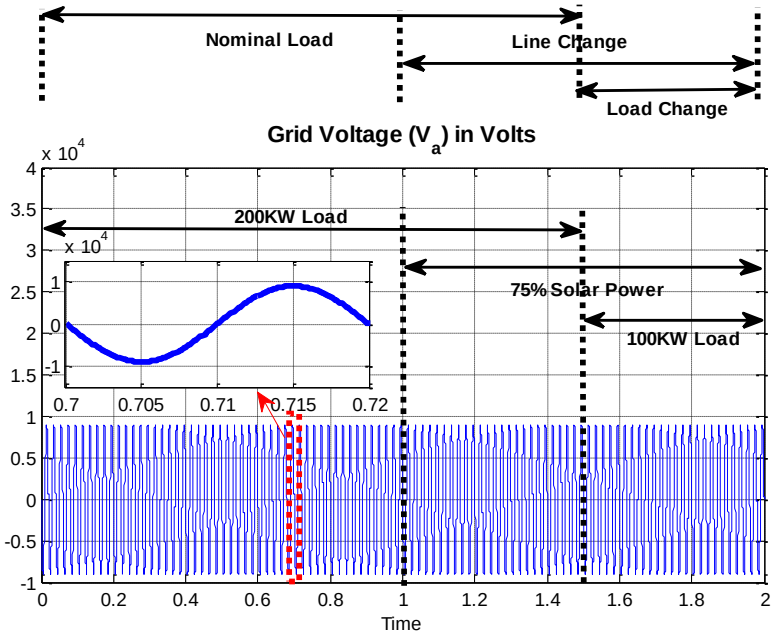


Figure 4.30. Grid voltage under load and line changes

The flow of current is explained in Fig. 4.29, while the grid voltage variation is shown in Fig. 4.30. A clear picture of the solar inverter/converter system emerges when comparison is made between the flow of voltage and current in the grid.

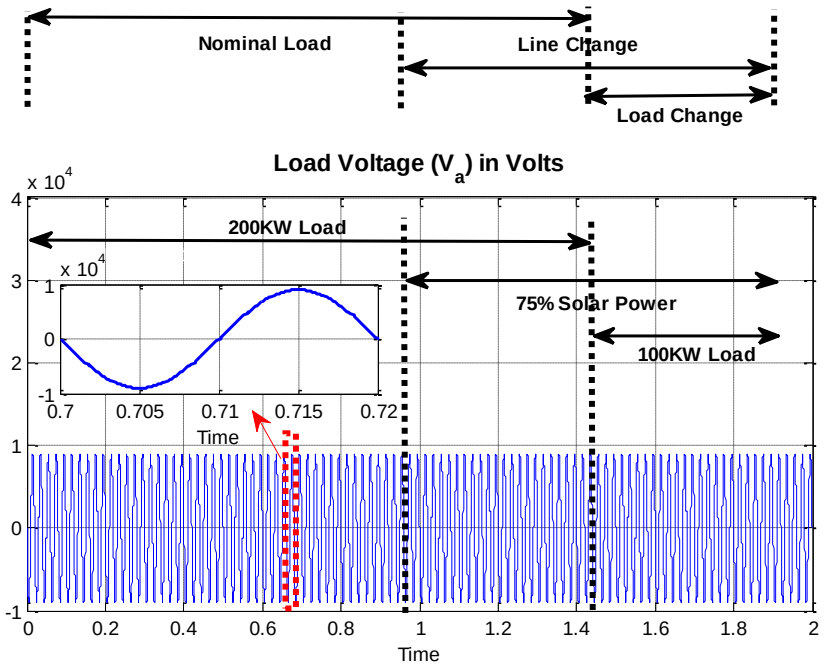


Figure 4.31. Load voltage under load and line changes.

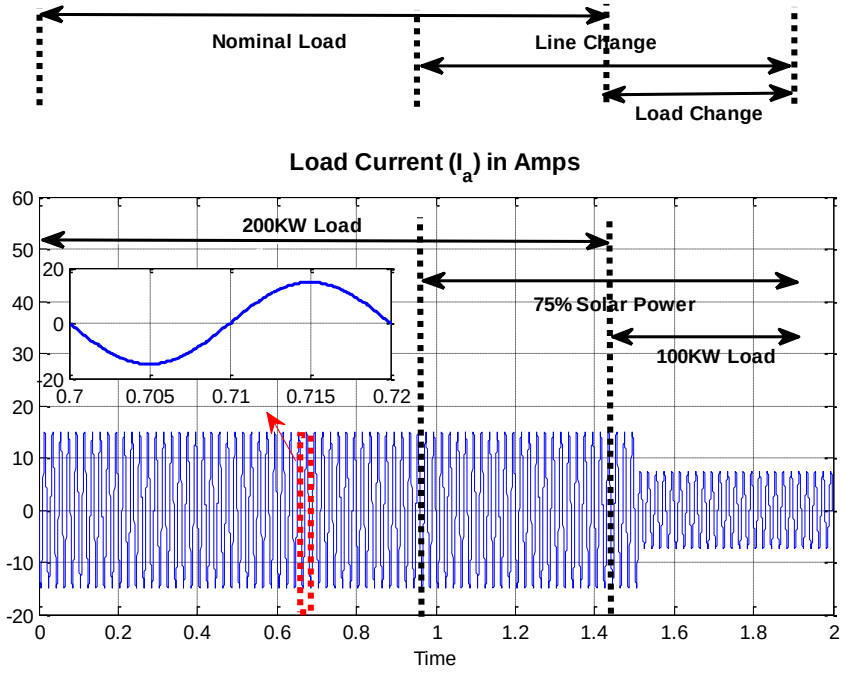


Figure 4.32. Load current under load and line changes.

Figure 4.31 represents the load voltage sharing in correspondence with line and load change against the nominal load which is a fixed point. Load current in Ampere is presented in Figure 4.32.

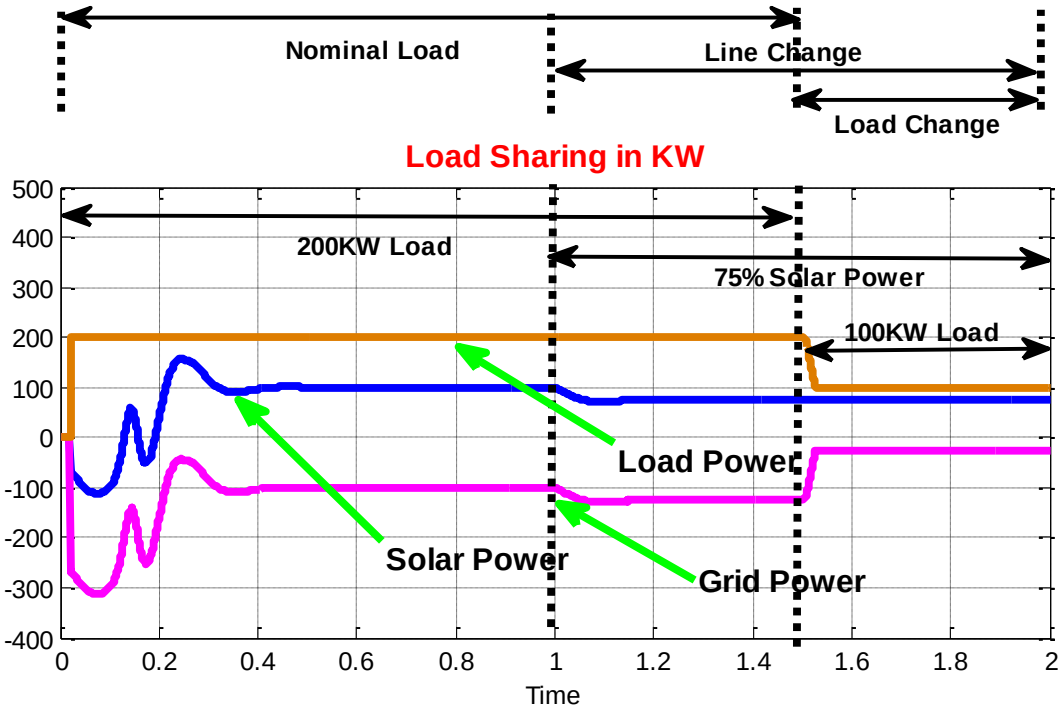


Figure 4.33. Load sharing in kW under load and line changes.

In Fig. 4.33, load sharing among PV and grid is demonstrated. When the load increases, dependence on grid power increases; when the load is less, dependence on solar power decreases. The gap and impact of line change and load change is also shown.

Power quality comparison of voltage and current waveforms are tabulated as shown in table 4.2.

| **THD(%) for Inverter output voltage** | | **THD(%) for Inverter current at PCC** | |
|---|---|---|---|
| 2-Level | 3-Level | 2-Level | 3-Level |
| 35.08 | 12.03 | 1.68 | 0.94 |

Table 4.2. THD comparison of Two-level and Three-level inverter topologies.

## 4.4. Conclusion

From the results obtained from simulation of both the inverter topologies, we can infer that the PV grid connected system is performing as expected. Appropriate load sharing

is demonstrated under varying timeline of conditions. Following are the main inferences from the simulations:

- Most essential requirement for a grid connected system is the maintenance of voltage at the point of common coupling. This has been achieved in the simulations for both topologies.
- Quick response of inverter output currents, modulation index and other system quantities to changing load conditions and PV output power are observed.
- Another important feature of grid integrated inverter is unity power factor operation, which is demonstrated by direct axis currents and voltage waveforms.
- Output inverter voltage and Injected inverter current waveforms are observed to show promising waveform power quality as shown in table 4.2. Three level topologies is superior in performance but costly at the same time due to the presence of more number of components (extra power diodes, switches, and input capacitor used).
- Synchronization of grid current and voltage is observed, as expected. Load sharing between grid and PV generator is also demonstrated.

# Chapter 5: HARDWARE SETUP

A laboratory prototype of grid connected photovoltaic system is designed for experimentation. Two level voltage fed inverter has been developed using a three phase bridge. A boost converter is used to step up the voltage output of installed photovoltaic modules.

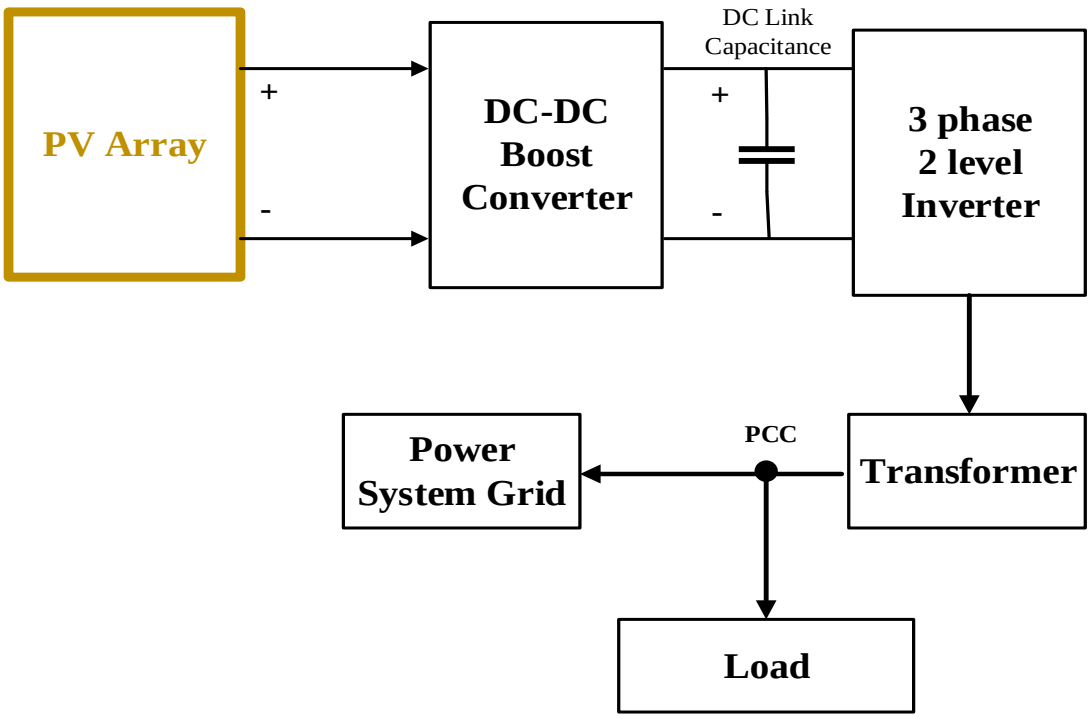


Figure 5.1. Schematic of system hardware for grid connected system.

The complete schematic diagram of the system is shown in figure 5.1. The experimental setup developed constitutes the following basic components:

- Power circuit of the Boost Converter and Three Phase Two Level Voltage Source Inverter.
- Measurement of system parameters, like PV voltage, PV current, Boost converter output voltage and inverter output voltages and currents.

- Development of power supplies.

System hardware is developed mainly in three stages

- Fabrication of the power circuit,
- Measurement of system parameters, and
- Testing of different components.

## 5.1. Power circuit components

### 5.1.1. Power circuit of three phase inverter

A voltage source converter with a suitably designed inductors on its AC side is used as an interface between DC link and the grid. The hardware prototype of three phase inverter is as shown in the figure 5.2. The SPWM controlled inverter consists of six self-commutated semiconductor switches ($S_1$ to $S_6$) with diodes ($D_1$ to $D_6$) connected in anti-parallel fashion. They may be realized using power transistors, MOSFETs and IGBTs based on the voltage ratings. MOSFETs IRF 460,(20A,500V at $20^0$C), with built-in fast recovery diodes are used as switching devices, featuring easy availability as well as low cost. Devices are mounted on a suitable heat sink to ensure proper heat dissipation. To achieve surge protection, snubber circuit is connected across each device.

Figure 5.2. Hardware prototype of three phase two level inverter.

### 5.1.2. Snubber Circuit

Voltage transients are introduced while switching high currents in short duration that could exceed the rating of the MOSFET. Therefore, snubbers are essential to protect the switches from transients. In figure 5.3, snubber circuit for MOSFET is shown. Discharging of the capacitor via the switching device is prevented by the diode, thus preventing damage of the device due to large discharge current. To protect against over-voltages across the devices, an additional protective metal oxide varistor (MOV) is used across each device.

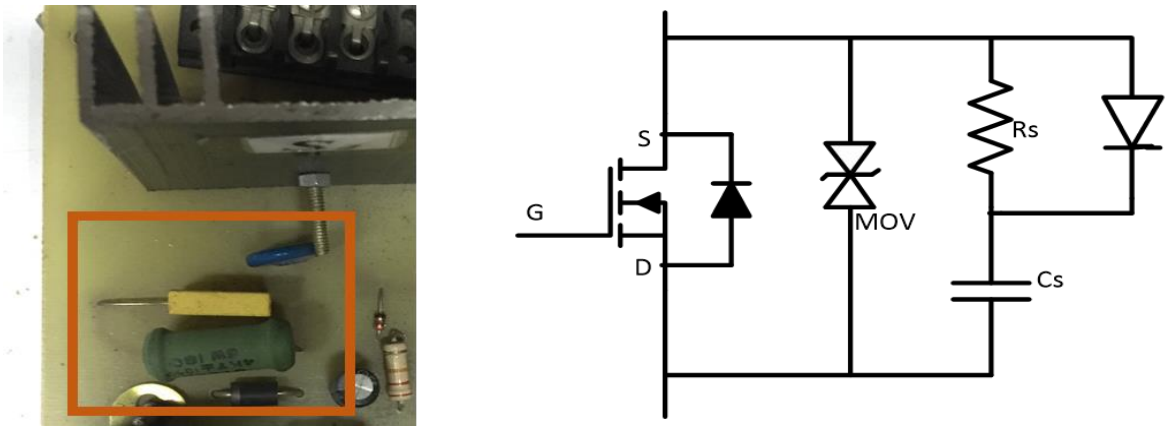


Figure 5.3. Snubber circuit for MOSFET protection (right) and its hardware implementation (left).

## 5.2. Measurement of system parameters

To achieve accurate and reliable operation of a system in closed loop, measurement and conditioning of various system parameters is essential, which must meet the following requirements:

- High accuracy
- Galvanic isolation from power circuit
- Linearity and fast response.
- Ease of installation

Due to the availability of Hall Effect current sensors and voltage sensors, these requirements are practically met to a great extent. To meet the system requirements, a variety of these sensors are available of required range and rating. Following signals are to be sensed in order to implement the control algorithm

- DC source voltage and DC current from PV arrays are required to track the maximum power point of PV panels. Also, DC link voltage is required to be sensed.

- AC grid side voltages are required to implement control loops, and
- AC grid side currents are required for comparison with generated current references.

### 5.2.1. AC current sensing

AC grid side currents are sensed using PCB mounted Hall Effect current sensors (ABB EL25P1). Galvanic isolation between high voltage power circuit and the low voltage control circuit is realized using the current sensor. This sensor require a nominal supply voltage of the ±12V to ±15V. It has the transformation ratio of 1000:1; hence its output is scaled appropriately to obtain the desired value as per the control requirements.

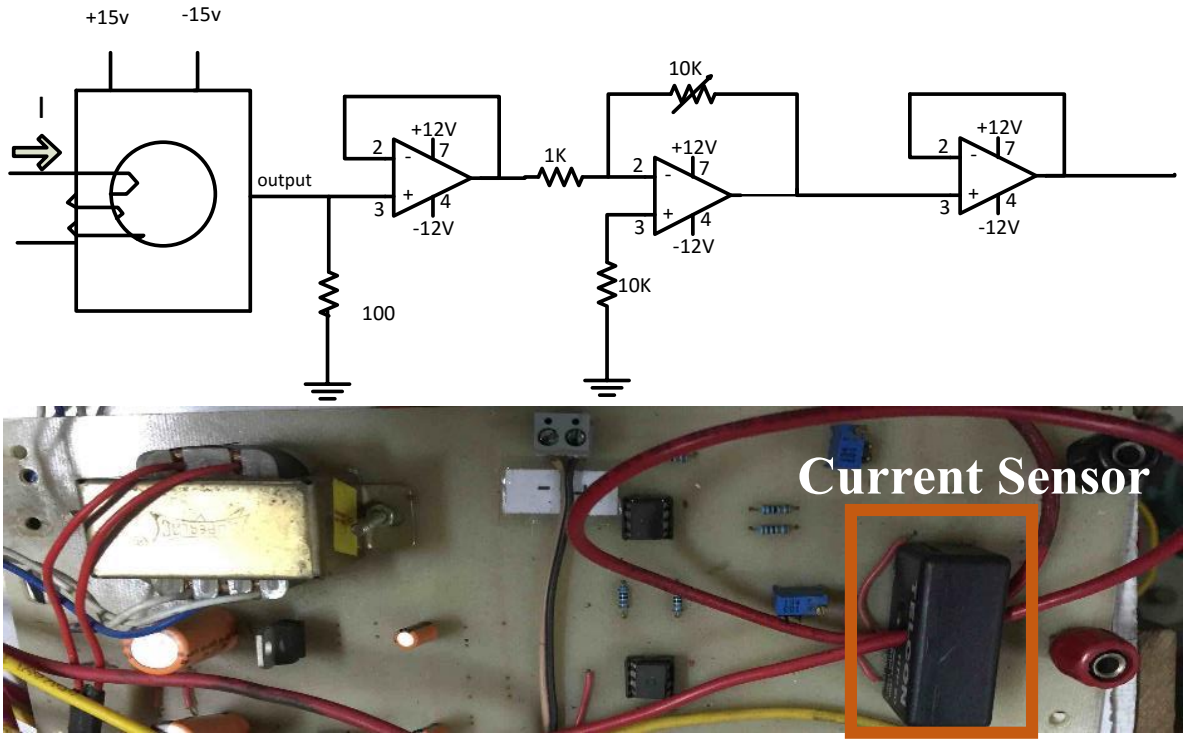


Figure 5.4. AC current sensor circuit.

### 5.2.2 AC voltage sensing

AC grid side voltages $v_a$, $v_b$ and $v_c$ (phase to neutral) are required to generate the current references. Sensing of two voltages is sufficient for three phase three wire system, rather all the three voltages are sensed in order to avoid the delay introduced due to the subtraction circuit. The circuit diagram of AC voltage sensing is as shown in the figure 5.5. Appropriate resistor values are designed to scale down the voltage within the operating range of AD202 (isolation amplifier). For scaling purpose, op-amp circuit using op-amp 741 IC are used at the output of AD202.

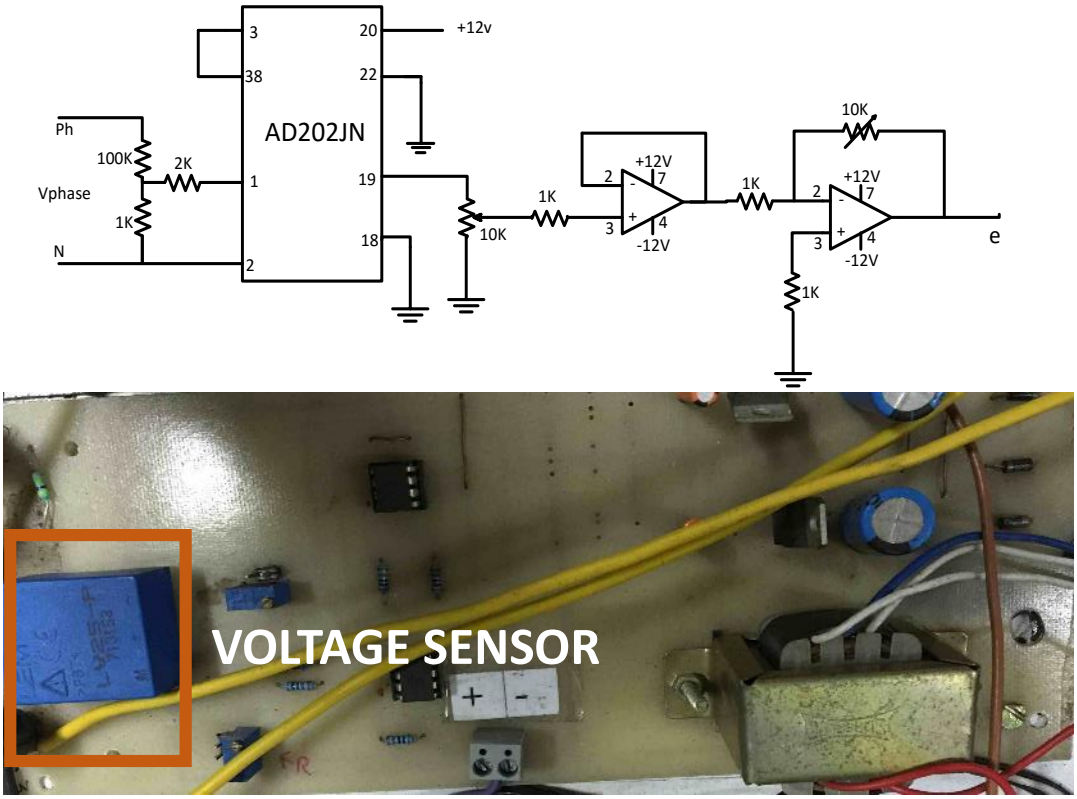


Figure 5.5. AC voltage sensing circuit

### 5.2.3 DC voltage sensing

DC link voltage is required to generate quadrature axis current when compared with the reference DC link voltage. Output voltage from PV panels is sensed to realize maximum power point tracking of PV panels. This voltage is measured by the isolation amplifier AD202. It operates using nominal supply voltage range of ±12V to ±15V. Output of the AD202 is scaled appropriately in order to match the control requirement. The circuit diagram of the DC voltage sensing is shown in the figure 5.6.

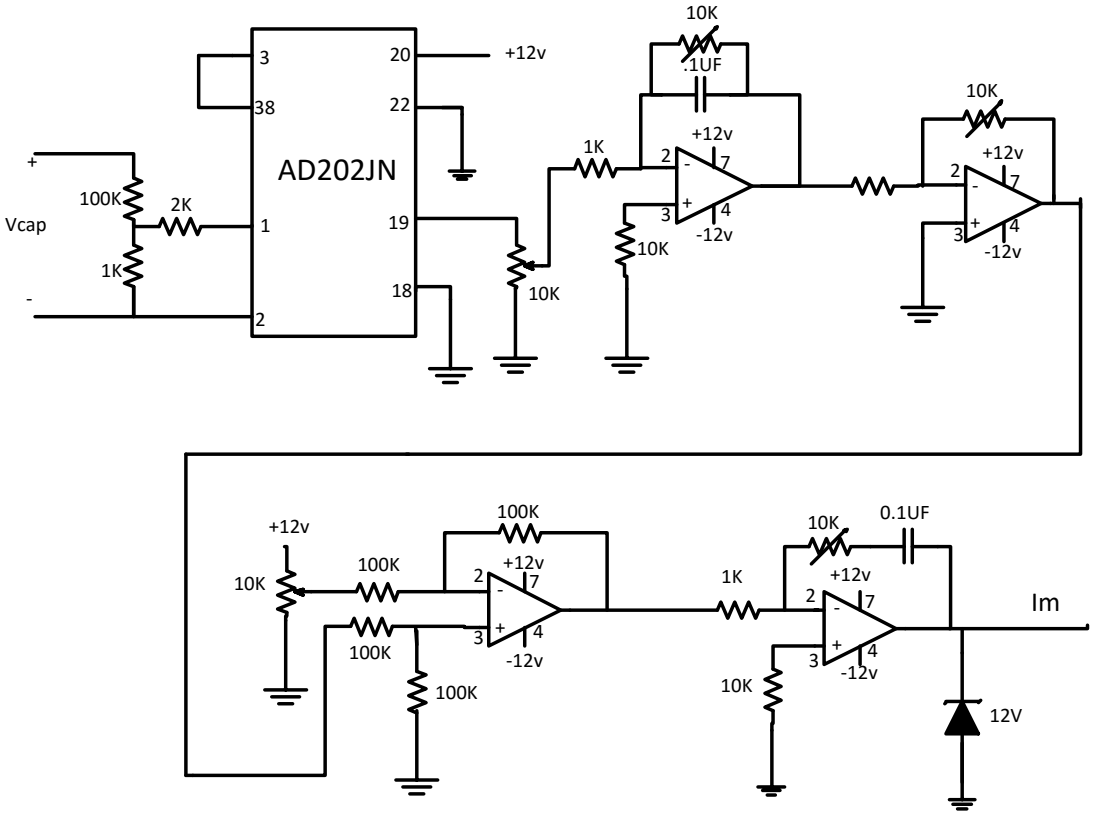


Figure 5.6. Circuit diagram of DC voltage controller with PI controller

## 5.3. Control hardware

### 5.3.1. Pulse amplification and isolation circuit

In **Figure**, the pulse amplification circuit for MOSFET is shown. The opto-coupler IC (MCT-2E) provides necessary isolation between the low voltage firing circuit and high voltage power circuit. The pulse amplification is realized using the output amplifier transistor (2N2222). When the input gating is +5V level, the transistor operates in saturation mode, forward biasing the LED, resulting in light emission. Falling of light on the base of phototransistor switches it by acting as its base drive. The output transistor is driven to cut off state and a +12V pulse (amplified) appears at its collector terminal.

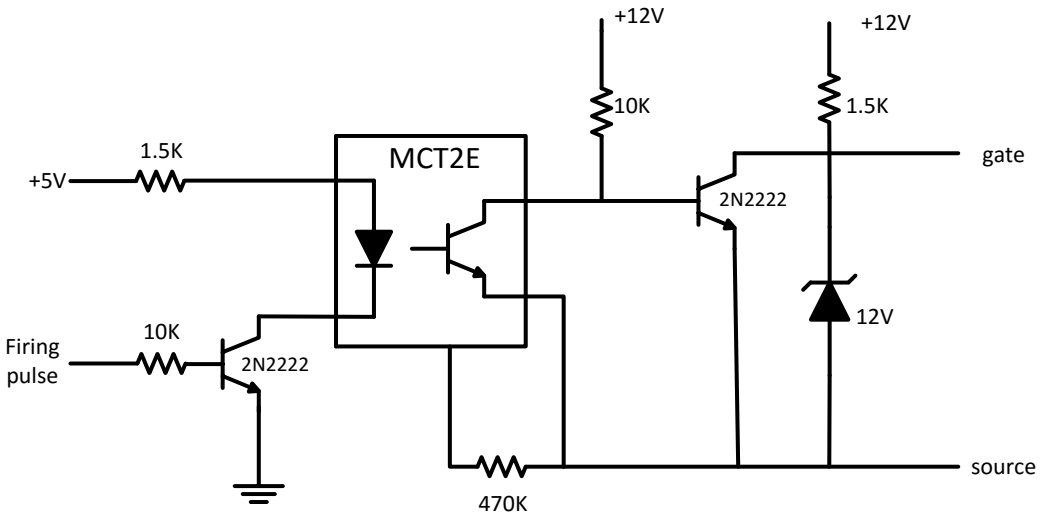


Figure 5.7. Pulse Amplification and Isolation Circuit

When the input gating pulse goes to ground level, the input switching transistor is cut-off and LED remains off, thus emitting no light, rendering the photo-transistor inactive. The output transistor receives base drive and goes to saturation mode, hence the output falls to ground level. Therefore, the circuit provides appropriate amplification and isolation.

Since slightest spike above 20V is capable of damaging the MOSFET, a 12V Zener diode is connected across the output isolation circuit. It clamps the triggering voltage to 12V.

### 5.3.2. Controller realization and PWM generation

FPGA SPARTAN 3E is used to generate control pulses to test different system components. Figure 5.8 shows the FPGA kit used in the realization for SPWM control of three phase two level inverter. As shown in figure 5.9, three gate pulses to control the inverter are generated.


Figure 5.8. FPGA SPARTAN 3E for control signals generation.

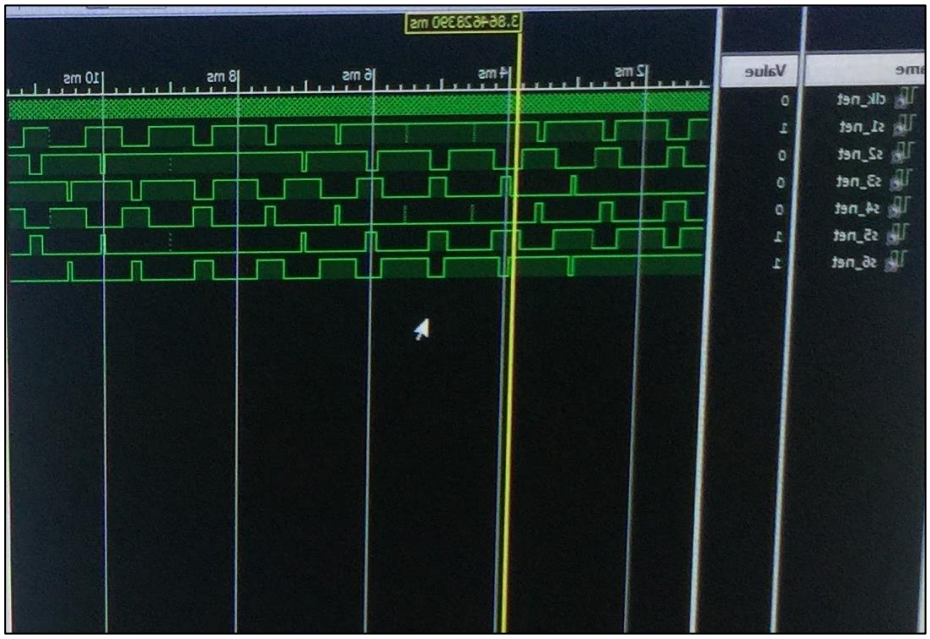

Figure 5.9. Gate Pulses for control of three phase two level inverter.

## 5.4. Power supplies

DC regulated supplies (+12V, GND, -12V, +5V) are required for providing biasing to various circuits like voltage and current detectors, pulse amplification and isolation

circuits. IC 7812 is used for +12V generation, IC 7912 for -12V and 7805 for +5V. The circuit diagram of the power supplies is as shown in following figures.

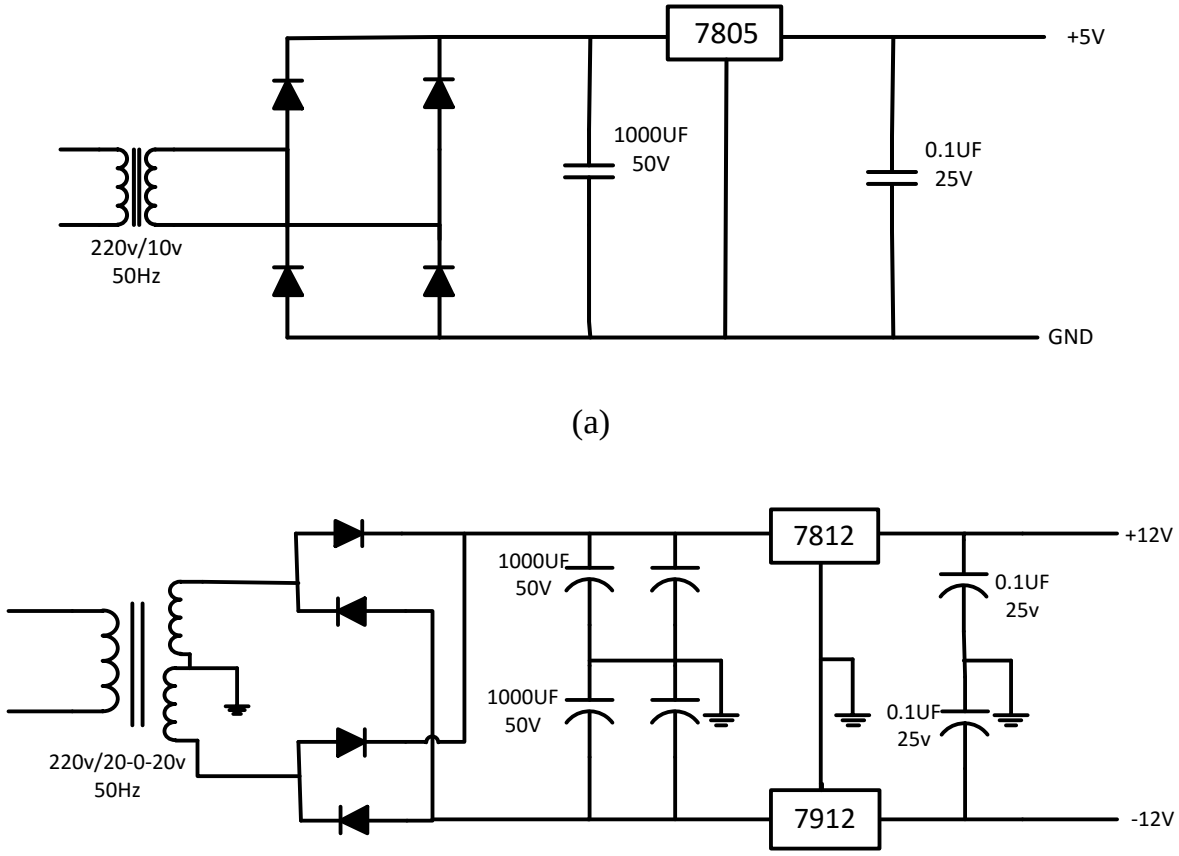


Figure 5.10. Connection diagram for power supplies (a) +5V (b)-12V, 0, +12V.

## 5.5. Testing of three phase inverter

Three phase two level inverter has been tested using three phase R load as the output. A rectifier is used to convert AC mains voltage to DC voltage, to be used as input to the inverter after the boost converter. The inverter is operated at 30 V line to line voltage (rms). The output voltage, $V_{ab}$ is shown in the figure 5.12, while complete testing setup is shown in figure 5.11.

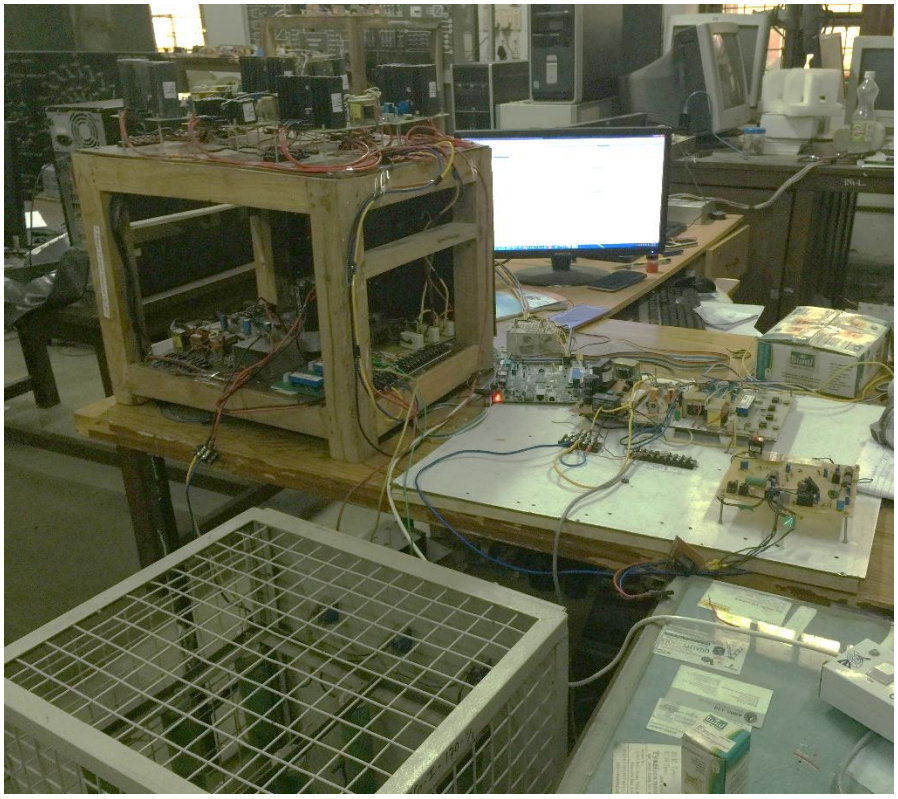

Figure 5.11. Testing setup for three phase bridge inverter.

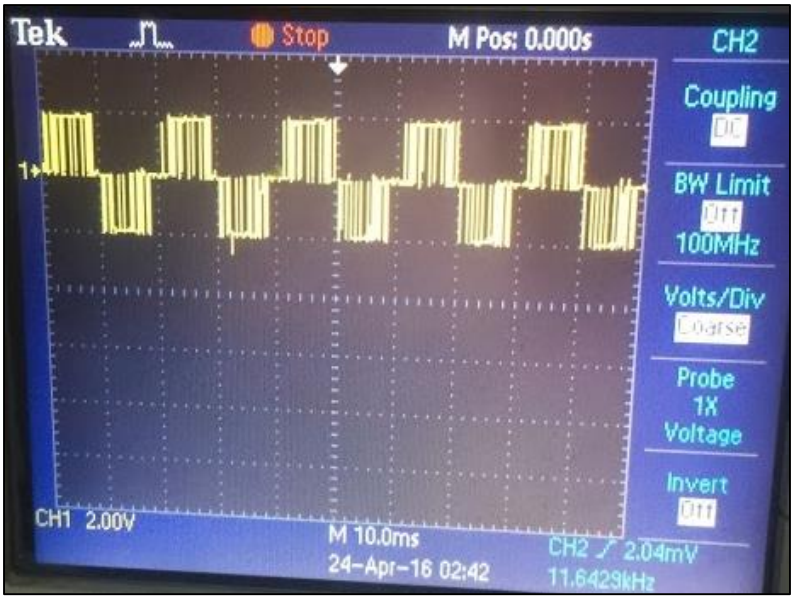


Figure 5.12. Inverter output voltage, Vab.

# Chapter 6: CONCLUSION AND RECOMMENDATIONS

Two VSI topologies chosen for grid connected photovoltaic system have been investigated successfully. As a part of a dual power stage grid connected PV system, performance, both the topologies are performing satisfactory as shown by the simulation results. The objective mentioned in the first chapter have been attained. Following are the contributions of this thesis:

- Study of two level and three level VSI topologies, system components and control structures to be used.
- Modeling of the PV array to study the various characteristics of the PV along with algorithms to extract the maximum power from the PV panel under varying environmental conditions of irradiance and temperature.
- Study of control strategy for three phase grid connected PV system including control of grid voltages and injected currents, and generating gating pulses for inverters.
- Simulations of the developed systems using MATLAB Simulink environment. Investigation of inverter performance for both topologies using customized simulation timeline of events.
- And, attempt to develop a hardware prototype of three phase grid connected PV system using two level inverter. Different components of the system are tested, and closed of operation of the system is recommended as the future work.

Apart from the two topologies taken in this work, there are also other single stage topologies that achieve boosting of PV voltage without the use of bulky switches, such as Z-source and quasi-Z-source inverters. Being a very wide topic, this application of renewable energy is full of possibilities.

# REFERENCES


[1] V. Lughi, A. M. Pavan, S. Quaia, G. Sulligoi, “Economical analysis and innovative solutions for grid connected PV plants,” in Proc. International Symposium on Power Electronics, Electrical Drives, Automation and Motion,. SPEEDAM 2008 pp: 211-216, 11-13 Jun 2008.

[2] “World Population to 2300” United Nation, N.Y.2004.

[3] F. Blaabjerg, Z. Chen, and S. Kjaer, “Power electronics as efficient interface in dispersed power generation systems,” IEEE Trans. Power Electron., vol. 19, no. 5, pp. 1184–1194, Sep. 2004.

[4] T. Key, “Finding a bright spot-- Utility experience, challenges, and opportunities in Photovoltaic Power,” IEEE Power and Energy Magazine, vol. 7, Issue 3, pp. 34 – 44, May-Jun 2009.

[5] L. Freris and D. Infield, Renewable Energy in Power Systems. 2008, John Wiley & Sons, Ltd.

[6] J. P. Benner and L. Kazmerski, “Photovoltaics gaining greater visibility,”IEEE Spectr., vol. 29, no. 9, pp. 34–42, Sep. 1999.

[7] M. G. Villalva, et al., "Comprehensive Approach to Modeling and Simulation of Photovoltaic Arrays," IEEE Transactions on Power Electronics, vol. 24, pp. 1198-1208, 2009.

[8] T. Esram and P. L. Chapman, "Comparison of Photovoltaic Array Maximum Power Point Tracking Techniques," IEEE Transactions on Energy Conversion, vol. 22, pp. 439-449, 2007.

[9] Hussein, K.H; Muta I; Hoshino, T; Osakada, M. "Maximum photovoltaic power tracking: an algorithm for rapidly changing atmospheric conditions," IEE Proceedings on Generation, Transmission and Distribution, vol.142, no.1, pp.59-64, Jan 1995.

[10] K. Kobayashi, I. Takano, and Y. Sawada, “A study on a two stage maximum power point tracking control of a photovoltaic system under partially shaded insolation conditions,” in IEEE Power Eng. Soc. Gen. Meet., 2003, pp. 2612–2617.

[11] Cuk, S. and Middlebrooks, Modeling, analysis and design of switching converters.

[12] “IEEE Recommended Practice for Utility Interface of Photovoltaic (PV) Systems," IEEE Std 929-2000, p.i, 2000.

[13] Kroutikova, N.; Hernandez-Aramburo, C.A.; Green, T.C.;, "State-space model of grid-connected inverters under current control mode," Electric Power Applications, IET , vol.1, no.3, pp.329-338, May 2007.

[14] F. Blaabjerg, et al., "Overview of Control and Grid Synchronization for Distributed Power Generation Systems," IEEE Transactions on Industrial Electronics, vol. 53, pp. 1398-1409, 2006.

[15] M. Marei, E. El-Saadany, and M. Salama, “A novel control algorithm for the DG interface to mitigate power quality problems," IEEE Transactions on Power Delivery, vol. 19, pp. 1384-1392, July 2004.

[16] F. Katiraei and M. R. Iravani, “Power management strategies for a microgird with multiple distributed generation units," IEEE Transactions on Power Systems, vol. 21, pp. 1821-1831, Nov. 2006.

[17] M. P. Kazmierkowski and L. Malesani, "Current control techniques for three-phase voltage source PWM converters: a survey," IEEE Transactions on Industrial Electronics, vol. 45, pp. 691-703, 1998.

[18] Y. Mohamed and E. F. El-Saadany, "Adaptive Decentralized Droop Controller to Preserve Power Sharing Stability of Paralleled Inverters in Distributed Generation Microgrids," IEEE Transactions on Power Electronics, vol. 23, pp. 2806-2816, 2008.

[19] A. Timbus, et al., "Evaluation of Current Controllers for Distributed Power Generation Systems," IEEE Transactions on Power Electronics, vol. 24, pp. 654-664, 2009.